

Clustering in Hilbert's Projective Geometry: The Case Studies of the Probability Simplex and the Elliptope of Correlation Matrices



Frank Nielsen and Ke Sun

Abstract Clustering categorical distributions in the probability simplex is a fundamental task met in many applications dealing with normalized histograms. Traditionally, differential-geometric structures of the probability simplex have been used either by (i) setting the Riemannian metric tensor to the Fisher information matrix of the categorical distributions, or (ii) defining the dualistic information-geometric structure induced by a smooth dissimilarity measure, the Kullback–Leibler divergence. In this work, we introduce for this clustering task a novel computationally-friendly framework for modeling the probability simplex termed *Hilbert simplex geometry*. In the Hilbert simplex geometry, the distance function is described by a polytope. We discuss the pros and cons of those different statistical modelings, and benchmark experimentally these geometries for center-based k -means and k -center clusterings. Furthermore, since a canonical Hilbert metric distance can be defined on any bounded convex subset of the Euclidean space, we also consider Hilbert's projective geometry of the elliptope of correlation matrices and study its clustering performances.

Keywords Fisher-Riemannian geometry · Information geometry
Multinoulli distribution · Hilbert simplex geometry · Polytope distance
Elliptope · Finsler geometry · k -means clustering · k -center clustering

F. Nielsen (✉)
Sony Computer Science Laboratories, Tokyo, Japan
e-mail: Frank.Nielsen@acm.org

K. Sun
CSIRO Data61, Sydney, Australia
e-mail: Ke.Sun@data61.csiro.au

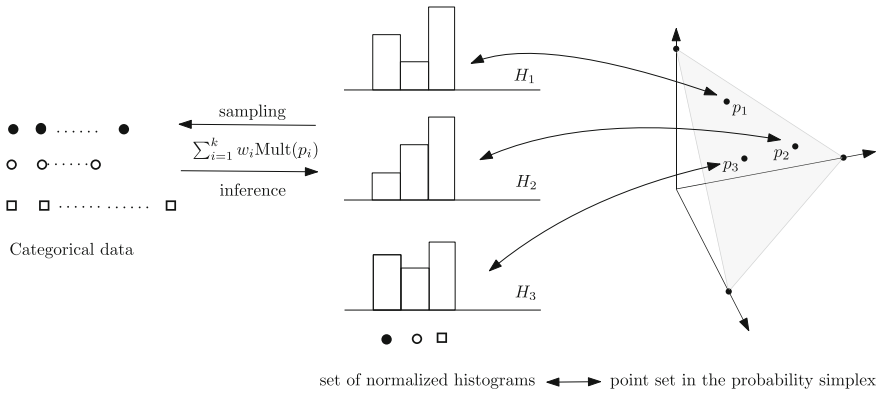


Fig. 1 Categorical datasets modeled by a generative statistical mixture model of multinoulli distributions can be visualized as a weighted set of normalized histograms or equivalently by a weighted point set encoding multinoulli distributions in the probability simplex Δ^d (here, $d = 2$ for trinoulli distributions — trinomial distributions with a single trial)

1 Introduction and Motivation

The categorical distributions and multinomial distributions are important probability distributions often met in data analysis [1], text mining [2], computer vision [3] and machine learning [4]. A multinomial distribution over a set $\mathcal{X} = \{e_0, \dots, e_d\}$ of outcomes (e.g., the $d + 1$ distinct colored faces of a die) is defined as follows: Let $\lambda_p^i > 0$ denote the probability that outcome e_i occurs for $i \in \{0, \dots, d\}$ (with $\sum_{i=0}^d \lambda_p^i = 1$). Denote by m the total number of events, with m_i reporting the number of outcome e_i . Then the probability $\Pr(X_0 = m_0, \dots, X_d = m_d)$ that a multinomial random variable $X = (X_0, \dots, X_d) \sim \text{Mult}(p = (\lambda_p^0, \dots, \lambda_p^d), m)$ (where X_i count the number of events e_i , and $\sum_{i=0}^d m_i = m$) is given by the following probability mass function (pmf):

$$\Pr(X_0 = m_0, \dots, X_d = m_d) = \frac{m!}{\prod_{i=0}^d m_i!} \prod_{i=0}^d (\lambda_p^i)^{m_i}.$$

The multinomial distribution is called a binomial distribution when $d = 1$ (e.g., coin tossing), a Bernoulli distribution when $m = 1$, and a “multinoulli distribution” (or categorical distribution) when $m = 1$ and $d > 1$. The multinomial distribution is also called a generalized Bernoulli distribution. A random variable X following a multinoulli distribution is denoted by $X = (X_0, \dots, X_d) \sim \text{Mult}(p = (\lambda_p^0, \dots, \lambda_p^d))$. The multinomial/multinoulli distribution provides an important *feature representation* in machine learning that is often met in applications [5–7] as normalized histograms (with non-empty bins) as illustrated in Fig. 1.

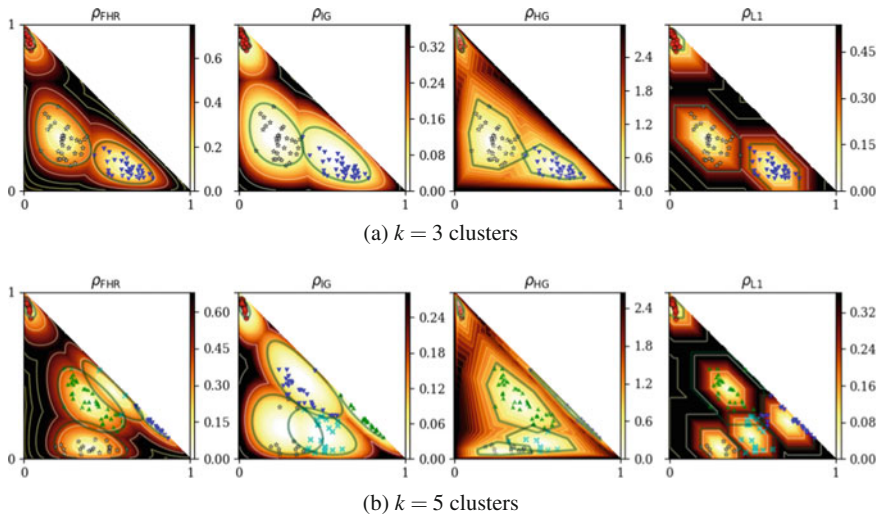


Fig. 2 Visualizing some k -center clustering results on a toy dataset in the space of trinomials Δ^2 for the considered four types of distances (and underlying geometries): Fisher-Hotelling-Rao metric distance (Riemannian geometry), Kullback–Leibler non-metric divergence (information geometry), Hilbert metric distance (Hilbert projective geometry), and total variation/ L_1 metric distance (norm geometry). Observe that the L_1 balls have hexagonal shapes on the probability simplex (intersection of a rotated cube with the plane H_{Δ^d}). The color density maps indicate the distance from any point to its nearest cluster center

A multinomial distribution $p \in \Delta^d$ can be thought as a point lying in the probability simplex Δ^d (standard simplex) with coordinates $p = (\lambda_p^0, \dots, \lambda_p^d)$ such that $\lambda_p^i = \Pr(X = e_i) > 0$ and $\sum_{i=0}^d \lambda_p^i = 1$. The open probability simplex Δ^d can be embedded in \mathbb{R}^{d+1} on the hyperplane $H_{\Delta^d} : \sum_{i=0}^d x^i = 1$. Notice that observations with D categorical attributes can be clustered using k -mode [8] with respect to the Hamming distance. Here, we consider the different task of clustering a set $\Lambda = \{p_1, \dots, p_n\}$ of n categorical/multinomial distributions in Δ^d [5] using center-based k -means++ or k -center clustering algorithms [9, 10], which rely on a dissimilarity measure (loosely called distance or divergence when smooth) between any two categorical distributions. In this work, we mainly consider four distances with their underlying geometries: (1) Fisher-Hotelling-Rao distance ρ_{FHR} (spherical geometry), (2) Kullback–Leibler divergence ρ_{IG} (dually flat geometry), (3) Hilbert distance ρ_{HG} (generalize Klein’s hyperbolic geometry), and (4) the total variation/ L_1 distance (norm geometry). The geometric structures of spaces are necessary in algorithms, for example, to define midpoint distributions. Figure 2 displays the k -center clustering results obtained with these four geometries as well as the L_1 distance ρ_{L_1} normed geometry on toy synthetic datasets in Δ^2 . We shall now explain the Hilbert simplex geometry applied to the probability simplex, describe how to perform k -center clustering in Hilbert geometry, and report experimental results that demonstrate the

superiority of the Hilbert geometry when clustering multinomials and correlation matrices.

The rest of this paper is organized as follows: Sect. 2 formally introduces the distance measures in Δ^d . Section 3 introduces how to efficiently compute the Hilbert distance. Section 4 presents algorithms for Hilbert minimax centers and Hilbert center-based clustering. Section 5 performs an empirical study of clustering multinomial distributions, comparing Riemannian geometry, information geometry, and Hilbert geometry. Section 6 presents a second use case of Hilbert geometry in machine learning: clustering correlation matrices in the elliptope [11]. Finally, Sect. 7 concludes this work by summarizing the pros and cons of each geometry. Although some contents require prior knowledge on geometric structures, we will present the detailed algorithms so that the general audience can still benefit from this work.

2 Four Distances with their Underlying Geometries

2.1 Fisher-Hotelling-Rao Riemannian Geometry

The Rao distance between two multinomial distributions is [6, 12]:

$$\rho_{\text{FHR}}(p, q) = 2 \arccos \left(\sum_{i=0}^d \sqrt{\lambda_p^i \lambda_q^i} \right). \quad (1)$$

It is a Riemannian metric length distance (satisfying the symmetric and triangular inequality axioms) obtained by setting the metric tensor g to the *Fisher information matrix* (FIM) $\mathcal{I}(p) = (g_{ij}(p))_{d \times d}$ with respect to the coordinate system $(\lambda_p^1, \dots, \lambda_p^d)$, where

$$g_{ij}(p) = \frac{\delta_{ij}}{\lambda_p^i} + \frac{1}{\lambda_p^0}.$$

We term this geometry the *Fisher-Hotelling-Rao (FHR) geometry* [13–16]. The metric tensor g allows one to define an inner product on each tangent plane T_p of the probability simplex manifold: $\langle u, v \rangle_p = u^\top g(p)v$. When g is everywhere the identity matrix, we recover the Euclidean (Riemannian) geometry with the inner product being the scalar product: $\langle u, v \rangle = u^\top v$. The geodesics $\gamma(p, q; \alpha)$ are defined by the Levi-Civita metric connection [17, 18] that is derived from the metric tensor. The FHR manifold can be embedded in the positive orthant of an Euclidean d -sphere in \mathbb{R}^{d+1} by using the *square root representation* $\lambda \mapsto \sqrt{\lambda}$ [12]. Therefore the FHR manifold modeling of Δ^d has constant *positive* curvature: It is a spherical geometry restricted to the positive orthant with the metric distance measuring the arc length on a great circle.

2.2 Information Geometry

A divergence D is a smooth C^3 differentiable dissimilarity measure [19] that allows to define a dual structure in Information Geometry (IG), see [17, 18, 20]. A f -divergence is defined for a strictly convex function f with $f(1) = 0$ by:

$$I_f(p : q) = \sum_{i=0}^d \lambda_p^i f\left(\frac{\lambda_q^i}{\lambda_p^i}\right) \geq f(1) = 0.$$

It is a *separable* divergence since the d -variate divergence can be written as a sum of d univariate (scalar) divergences: $I_f(p : q) = \sum_{i=0}^d I_f(\lambda_p^i : \lambda_q^i)$. The class of f -divergences plays an essential role in information theory since they are provably the *only* separable divergences that satisfy the *information monotonicity* property [17, 21] (for $d \geq 2$). That is, by coarse-graining the histograms, we obtain lower-dimensional multinomials, say p' and q' , such that $0 \leq I_f(p' : q') \leq I_f(p : q)$ [17]. The Kullback–Leibler (KL) divergence ρ_{IG} is a f -divergence obtained for the functional generator $f(u) = -\log u$:

$$\rho_{IG}(p, q) = \sum_{i=0}^d \lambda_p^i \log \frac{\lambda_p^i}{\lambda_q^i}. \tag{2}$$

It is an asymmetric non-metric distance: $\rho_{IG}(p, q) \neq \rho_{IG}(q, p)$. In differential geometry, the structure of a manifold is defined by two independent components:

1. A *metric tensor* g that allows to define an inner product $\langle \cdot, \cdot \rangle_p$ at each tangent space (for measuring vector lengths and angles between vectors);
2. A *connection* ∇ that defines *parallel transport* \prod_c^∇ , i.e., a way to move a tangent vector from one tangent plane T_p to any other one T_q along a smooth curve c , with $c(0) = p$ and $c(1) = q$.

In FHR geometry, the implicitly-used connection is called the Levi-Civita connection that is induced by the metric g : $\nabla^{LC} = \nabla(g)$. It is a metric connection since it ensures that $\langle u, v \rangle_p = \langle \prod_{c(t)}^{\nabla^{LC}} u, \prod_{c(t)}^{\nabla^{LC}} v \rangle_{c(t)}$ for $t \in [0, 1]$. The underlying information-geometric structure of KL is characterized by a pair of *dual* connections [17] $\nabla = \nabla^{(-1)}$ (mixture connection) and $\nabla^* = \nabla^{(1)}$ (exponential connection) that induces a corresponding pair of dual geodesics (technically, ± 1 -autoparallel curves, [18]). Those connections are said *flat* as they define two dual global affine coordinate systems θ and η on which the θ - and η -geodesics are (Euclidean) straight line segments, respectively. For multinomials, the *expectation parameters* are: $\eta = (\lambda^1, \dots, \lambda^d)$ and they one-to-one correspond to the *natural parameters*: $\theta = \left(\log \frac{\lambda^1}{\lambda^0}, \dots, \log \frac{\lambda^d}{\lambda^0}\right) \in \mathbb{R}^d$. Thus in IG, we have two kinds of midpoint multinomials of p and q , depending on whether we perform the (linear) interpolation on the θ - or the η -geodesics. Informally speaking, the dual connections $\nabla^{(\pm 1)}$ are said coupled to the FIM since we have $\frac{\nabla + \nabla^*}{2} = \nabla(g) = \nabla^{LC}$. Those dual (torsion-free affine)

connections are not metric connections but enjoy the following metric-compatibility property when used together as follows: $\langle u, v \rangle_p = \langle \prod_{c(t)} u, \prod_{c(t)}^* v \rangle_{c(t)}$ (for $t \in [0, 1]$), where $\prod := \prod^\nabla$ and $\prod^* := \prod^{\nabla^*}$ are the corresponding induced dual parallel transports. The geometry of f -divergences [19] is the α -geometry (for $\alpha = 3 + 2f'''(1)$) with the dual $\pm\alpha$ -connections, where $\nabla^{(\alpha)} = \frac{1+\alpha}{2}\nabla^* + \frac{1-\alpha}{2}\nabla$. The Levi-Civita metric connection is $\nabla^{\text{LC}} = \nabla^{(0)}$. More generally, it was shown how to build a dual information-geometric structure for *any* divergence [19]. For example, we can build a dual structure from the symmetric Cauchy–Schwarz divergence [22]:

$$\rho_{\text{CS}}(p, q) = -\log \frac{\langle \lambda_p, \lambda_q \rangle}{\sqrt{\langle \lambda_p, \lambda_p \rangle \langle \lambda_q, \lambda_q \rangle}}. \tag{3}$$

2.3 Hilbert Simplex Geometry

In Hilbert geometry (HG), we are given a bounded convex domain \mathcal{C} (here, $\mathcal{C} = \Delta^d$), and the distance between any two points M, M' of \mathcal{C} is defined [23] as follows: Consider the two intersection points AA' of the line (MM') with \mathcal{C} , and order them on the line so that we have A, M, M', A' . Then the Hilbert metric distance [24] is defined by:

$$\rho_{\text{HG}}(M, M') = \begin{cases} \left| \log \frac{|A'M||AM'|}{|A'M'||AA'|} \right|, & M \neq M', \\ 0 & M = M'. \end{cases} \tag{4}$$

It is also called the Hilbert cross-ratio metric distance [25, 26]. Notice that we take the absolute value of the logarithm since the Hilbert distance is a *signed distance* [27]. When \mathcal{C} is the unit ball, HG lets us recover the Klein hyperbolic geometry [26]. When \mathcal{C} is a quadric bounded convex domain, we obtain the Cayley–Klein hyperbolic geometry [28] which can be studied with the Riemannian structure and the corresponding metric distance called the curved Mahalanobis distances [29, 30]. Cayley–Klein hyperbolic geometries have negative curvature. Elements on the boundary are called ideal elements [31].

In Hilbert geometry, the geodesics are *straight* Euclidean lines making them convenient for computation. Furthermore, the domain boundary $\partial\mathcal{C}$ needs not to be smooth: One may also consider bounded polytopes [32]. This is particularly interesting for modeling Δ^d , the d -dimensional open standard simplex. We call this geometry the *Hilbert simplex geometry* [33]. In Fig. 3, we show that the Hilbert distance between two multinomial distributions $p(M)$ and $q(M')$ can be computed by finding the two intersection points of the line $(1-t)p + tq$ with $\partial\Delta^d$, denoted as $t_0 \leq 0$ and $t_1 \geq 1$. Then

$$\rho_{\text{HG}}(p, q) = \left| \log \frac{(1-t_0)t_1}{(-t_0)(t_1-1)} \right| = \log \left(1 - \frac{1}{t_0} \right) - \log \left(1 - \frac{1}{t_1} \right).$$

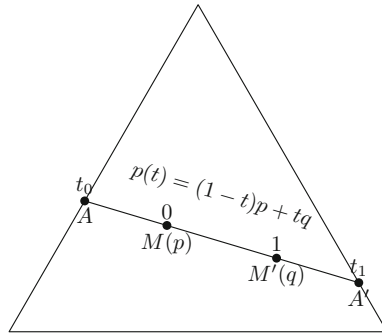


Fig. 3 Computing the Hilbert metric distance for trinomials on the 2D probability simplex as the logarithm of the cross ratio $(M, M'; A, A')$ of the four collinear points A, M, M' and A'

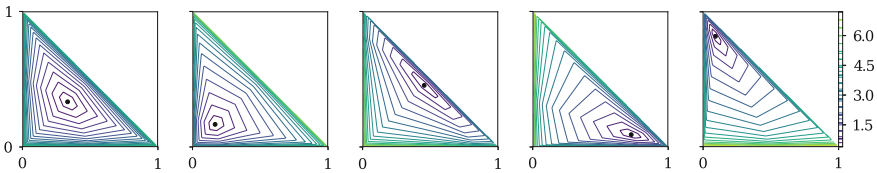


Fig. 4 Balls in the Hilbert simplex geometry Δ^2 have polygonal Euclidean shapes of constant combinatorial complexity. At infinitesimal scale, the balls have hexagonal shapes, showing that the Hilbert geometry is not Riemannian

The shape of balls in polytope-domain HG is Euclidean polytopes¹ [26], as depicted in Fig.4. Furthermore, the Euclidean shape of the balls does not change with the radius. Hilbert balls have hexagons shapes in 2D [34], rhombic dodecahedra shapes in 3D, and are polytopes [26] with $d(d + 1)$ facets in dimension d . When the polytope domain is not a simplex, the combinatorial complexity of balls depends on the center location [34], see Fig.5. The HG of the probability simplex yields a non-Riemannian geometry, because, at an infinitesimal radius, the balls are polytopes and not ellipsoids (corresponding to squared Mahalanobis distance balls used to visualize metric tensors [35]). The isometries in Hilbert polyhedral geometries are studied in [36]. In Appendix 9, we recall that any Hilbert geometry induces a Finslerian structure that becomes Riemannian iff the boundary is an ellipsoid (yielding the hyperbolic Cayley–Klein geometries [27]). Notice that in Hilbert simplex/polytope geometry, the geodesics are not unique (see Figure 2 of [25]).

¹To contrast with this result, let us mention that infinitesimal small balls in Riemannian geometry have Euclidean ellipsoidal shapes (visualized as Tissot’s indicatrix in cartography).

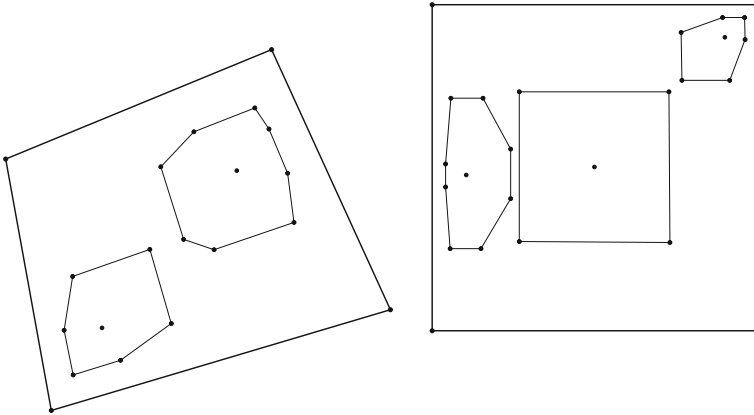


Fig. 5 Hilbert balls in quadrangle domains have combinatorial complexity depending on the center location

2.4 L_1 -Norm Geometry

The Total Variation (TV) metric distance between two multinomials p and q is defined by:

$$\text{TV}(p, q) = \frac{1}{2} \sum_{i=0}^d |\lambda_p^i - \lambda_q^i|.$$

It is a statistical f -divergence obtained for the generator $f(u) = \frac{1}{2}|u - 1|$. The L_1 -norm induced distance ρ_{L1} (L1) is defined by:

$$\rho_{L1}(p, q) = \|\lambda_p - \lambda_q\|_1 = \sum_{i=0}^d |\lambda_p^i - \lambda_q^i| = 2\text{TV}(p, q).$$

Therefore the distance ρ_{L1} satisfies information monotonicity (for coarse-grained histograms p' and q' of $\Delta^{D'}$ with $D' < D$):

$$0 \leq \rho_{L1}(p', q') \leq \rho_{L1}(p, q).$$

For trinomials, the ρ_{L1} distance is given by:

$$\rho_{L1}(p, q) = |\lambda_p^0 - \lambda_q^0| + |\lambda_p^1 - \lambda_q^1| + |\lambda_q^0 - \lambda_p^0 + \lambda_q^1 - \lambda_p^1|.$$

The L_1 distance function is a polytopal distance function described by the dual polytope \mathcal{Z} of the d -dimensional cube called the standard (or regular) d -cross-polytope [37], the orthoplex [38] or the d -cocube [39]: The cross-polytope \mathcal{Z} can be obtained as the convex hull of the $2d$ unit standard base vectors $\pm e_i$ for

Table 1 Comparing the geometric modelings of the probability simplex Δ^d

	Riemannian Geometry	Information Rie. Geo.	Non-Rie. Hilbert Geo.
Structure	$(\Delta^d, g, \nabla^{LC} = \nabla(g))$	$(\Delta^d, g, \nabla^{(\alpha)}, \nabla^{(-\alpha)})$	(Δ^d, ρ)
	Levi-Civita $\nabla^{LC} = \nabla^{(0)}$	Dual connections $\nabla^{(\pm\alpha)}$ so that $\frac{\nabla^{(\alpha)} + \nabla^{(-\alpha)}}{2} = \nabla^{(0)}$	Connection of \mathbb{R}^d
Distance	Rao distance (metric)	α -divergence (non-metric) KL or reverse KL for $\alpha = \pm 1$	Hilbert distance (metric)
Property	Invariant to reparameterization	Information monotonicity	Isometric to a normed space
Calculation	Closed-form	Closed-form	Easy (Algorithm 1)
Geodesic	Shortest path	Straight either in θ/η	Straight
Smoothness	Manifold	Manifold	Non-manifold
Curvature	Positive	Dually flat	Negative

$i \in \{0, \dots, d - 1\}$. The cross-polytope is one of the three regular polytopes in dimension $d \geq 4$ (with the hypercubes and simplices): It has $2d$ vertices and 2^d facets. Therefore the L_1 balls on the hyperplane H_{Δ^d} supporting the probability simplex is the intersection of a $(d + 1)$ -cross-polytope with d -dimensional hyperplane H_{Δ^d} . Thus the “multinomial ball” $\text{Ball}_{L_1}(p, r)$ of center p and radius r is defined by $\text{Ball}_{L_1}(p, r) = (\lambda_p \oplus r \mathcal{Z}) \cap H_{\Delta^d}$. In 2D, the shape of L_1 trinomial balls is that of a regular octahedron (twelve edges and eight faces) cut by the 2D plane H_{Δ^2} : Trinomial balls have hexagonal shapes as illustrated in Fig. 2 (for ρ_{L_1}). In 3D, trinomial balls are Archimedean solid cuboctahedra, and in arbitrary dimension, the shapes are polytopes with $d(d + 1)$ vertices [40]. Let us note in passing, that in 3D, the L_1 multinomial cuboctahedron ball has the dual shape of the Hilbert rhombic dodecahedron ball.

Table 1 summarizes the characteristics of the three main geometries: FHR, IG, and HG. Let us conclude this introduction by mentioning the Cramér–Rao lower bound and its relationship with information geometry [41]: Consider an unbiased estimator $\hat{\theta} = T(X)$ of a parameter θ estimated from measurements distributed according to a smooth density $p(x; \theta)$ (i.e., $X \sim p(x; \theta)$). The Cramér–Rao Lower Bound (CRLB) states that the variance of $T(X)$ is greater or equal to the inverse of the FIM $\mathcal{J}(\theta)$: $V_\theta[T(X)] \succ \mathcal{J}^{-1}(\theta)$. For regular parametric families $\{p(x; \theta)\}_\theta$, the FIM is a positive-definite matrix and defines a metric tensor, called the Fisher metric in Riemannian geometry. The FIM is the cornerstone of information geometry [17] but requires the differentiability of the probability density function (pdf).

A better lower bound that does not require the pdf differentiability is the Hammersley–Chapman–Robbins Lower Bound [42, 43] (HCRLB):

$$V_\theta[T(X)] \geq \sup_{\Delta} \frac{\Delta^2}{E_\theta \left[\left(\frac{p(x; \theta + \Delta) - p(x; \theta)}{p(x; \theta)} \right)^2 \right]}. \tag{5}$$

By introducing the χ^2 -divergence, $\chi^2(P : Q) = \int \left(\frac{dP-dQ}{dQ} \right)^2 dQ$, we rewrite the HCRLB using the χ^2 -divergence in the denominator as follows:

$$V_\theta[T(X)] \geq \sup_{\Delta} \frac{\Delta^2}{\chi^2(P(x; \theta + \Delta) : P(x; \theta))}. \tag{6}$$

Note that the FIM is not defined for non-differentiable pdfs, and therefore the Cramér–Rao lower bound does not exist in that case.

3 Computing Hilbert Distance in Δ^d

Let us start with the simplest case: The 1D probability simplex Δ^1 , the space of Bernoulli distributions. Any Bernoulli distribution can be represented by the activation probability of the random bit x : $\lambda = p(x = 1) \in \Delta^1$, corresponding to a point in the interval $\Delta^1 = (0, 1)$. We write the Bernoulli manifold as an exponential family as

$$p(x) = \exp(x\theta - F(\theta)), \quad x \in \{0, 1\},$$

where $F(\theta) = \log(1 + \exp(\theta))$. Therefore $\lambda = \frac{\exp(\theta)}{1 + \exp(\theta)}$ and $\theta = \log \frac{\lambda}{1-\lambda}$.

3.1 1D Probability Simplex of Bernoulli Distributions

By definition, the Hilbert distance has the closed form:

$$\rho_{\text{HG}}(p, q) = \left| \log \frac{\lambda_q(1 - \lambda_p)}{\lambda_p(1 - \lambda_q)} \right| = \left| \log \frac{\lambda_p}{1 - \lambda_p} - \log \frac{\lambda_q}{1 - \lambda_q} \right|.$$

Note that $\theta_p = \log \frac{\lambda_p}{1-\lambda_p}$ is the canonical parameter of the Bernoulli distribution.

The FIM of the Bernoulli manifold in the λ -coordinates is given by: $g = \frac{1}{\lambda} + \frac{1}{1-\lambda} = \frac{1}{\lambda(1-\lambda)}$. The FHR distance is obtained by integration as:

$$\rho_{\text{FHR}}(p, q) = 2 \arccos \left(\sqrt{\lambda_p \lambda_q} + \sqrt{(1 - \lambda_p)(1 - \lambda_q)} \right).$$

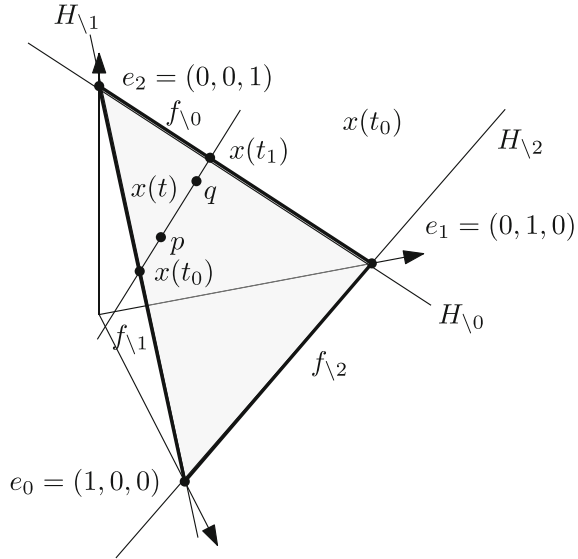
Notice that $\rho_{\text{FHR}}(p, q)$ has finite values on $\partial \Delta^1$.

The KL divergence of the ± 1 -geometry is:

$$\rho_{\text{IG}}(p, q) = \lambda_p \log \frac{\lambda_p}{\lambda_q} + (1 - \lambda_p) \log \frac{1 - \lambda_p}{1 - \lambda_q}.$$

The KL divergence belongs to the family of α -divergences [17].

Fig. 6 Calculating the two intersection points $x(t_0)$ and $x(t_1)$ of the line (pq) with the boundary of the probability simplex Δ_d : For each facet f_i , we calculate the intersection point of line $x(t) = (1 - t)p + tq$ with the d -dimensional hyperplane H_i supporting the facet f_i



3.2 Arbitrary Dimension Case

Given $p, q \in \Delta^d$, we first need to compute the intersection of line (pq) with the border of the d -dimensional probability simplex to get the two intersection points p' and q' so that p', p, q, q' are ordered on (pq) . Once this is done, we simply apply the formula in Eq. 4 to get the Hilbert distance.

A d -dimensional simplex consists of $d + 1$ vertices with their corresponding $(d - 1)$ -dimensional facets. For the probability simplex Δ^d , let $e_i = (\underbrace{0, \dots, 0}_i, 1, 0, \dots, 0)$

denote the $d + 1$ vertices of the standard simplex embedded in the hyperplane $H_\Delta : \sum_{i=0}^d \lambda^i = 1$ in \mathbb{R}^{d+1} . Let $f_{\setminus j}$ denote the simplex facets that is the convex hull of all vertices except e_j : $f_{\setminus j} = \text{hull}(e_0, \dots, e_{j-1}, e_{j+1}, \dots, e_d)$. Let $H_{\setminus j}$ denote the hyperplane supporting this facet, which is the affine hull $f_{\setminus j} = \text{affine}(e_0, \dots, e_{j-1}, e_{j+1}, \dots, e_d)$.

To compute the two intersection points of (pq) with Δ^d , a naive algorithm consists in computing the unique intersection point r_j of the line (pq) with each hyperplane $H_{\setminus j}$ ($j = 0, \dots, d$) and checking whether r_j belongs to $f_{\setminus j}$.

A much more efficient implementation given by Algorithm (1) calculates the intersection point of the line $x(t) = (1 - t)p + tq$ with each $H_{\setminus j}$ ($j = 0, \dots, d$). These intersection points are represented using the coordinate t . For example, $x(0) = p$ and $x(1) = q$. Due to convexity, any intersection point with $H_{\setminus j}$ must satisfy either $t \leq 0$ or $t \geq 1$. Then, the two intersection points with $\partial\Delta^d$ are obtained by $t_0 = \max\{t : \exists j, x(t) \in H_{\setminus j} \text{ and } t \leq 0\}$ and $t_1 = \min\{t : \exists j, x(t) \in H_{\setminus j} \text{ and } t \geq 1\}$. Figure 6 illustrates this calculation method. This algorithm only requires $O(d)$ time and $O(1)$ memory.

Lemma 1 *The Hilbert distance in the probability simplex can be computed in optimal $\Theta(d)$ time.*

Algorithm 1: Computing the Hilbert distance

Data: Two points $p = (\lambda_p^0, \dots, \lambda_p^d), q = (\lambda_q^0, \dots, \lambda_q^d)$ in the d -dimensional simplex Δ^d

Result: Their Hilbert distance $\rho_{HG}(p, q)$

```

1 begin
2    $t_0 \leftarrow -\infty; t_1 \leftarrow +\infty;$ 
3   for  $i = 0 \dots d$  do
4     if  $\lambda_p^i \neq \lambda_q^i$  then
5        $t \leftarrow \lambda_p^i / (\lambda_p^i - \lambda_q^i);$ 
6       if  $t_0 < t \leq 0$  then
7          $t_0 \leftarrow t;$ 
8       else if  $1 \leq t < t_1$  then
9          $t_1 \leftarrow t;$ 
10  if  $t_0 = -\infty$  or  $t_1 = +\infty$  then
11    Output  $\rho_{HG}(p, q) = 0;$ 
12  else if  $t_0 = 0$  or  $t_1 = 1$  then
13    Output  $\rho_{HG}(p, q) = \infty;$ 
14  else
15    Output  $\rho_{HG}(p, q) = \left| \log(1 - \frac{1}{t_0}) - \log(1 - \frac{1}{t_1}) \right|;$ 

```

Once an arbitrary distance ρ is chosen, we can define a ball centered at c and of radius r as $B_\rho(c, r) = \{x : \rho(c, x) \leq r\}$. Figure 4 displays the hexagonal shapes of the Hilbert balls for various center locations in Δ^2 .

Theorem 1 (Balls in a simplicial Hilbert geometry [26]) *A ball in the Hilbert simplex geometry has a Euclidean polytope shape with $d(d + 1)$ facets.*

Note that when the domain is not simplicial, the Hilbert balls can have varying combinatorial complexity depending on the center location. In 2D, the Hilbert ball can have $s \sim 2s$ edges inclusively, where s is the number of edges of the boundary of the Hilbert domain $\partial\mathcal{C}$.

Since a Riemannian geometry is locally defined by a metric tensor, at infinitesimal scales, Riemannian balls have Mahalanobis smooth ellipsoidal shapes: $B_\rho(c, r) = \{x : (x - c)^\top g(c)(x - c) \leq r^2\}$. This property allows one to visualize Riemannian metric tensors [35]. Thus we conclude that:

Lemma 2 ([26]) *Hilbert simplex geometry is a non-manifold metric length space.*

As a remark, let us notice that slicing a simplex with a hyperplane does not always produce a lower-dimensional simplex. For example, slicing a tetrahedron by a plane yields either a triangle or a quadrilateral. Thus the restriction of a d -dimensional ball B in a Hilbert simplex geometry Δ^d to a hyperplane H is a $(d - 1)$ -dimensional ball $B' = B \cap H$ of varying combinatorial complexity, corresponding to a ball in the induced Hilbert sub-geometry in the convex sub-domain $H \cap \Delta^d$.

3.3 Visualizing Distance Profiles

Figure 7 displays the distance profile from any point in the probability simplex to a fixed reference point (trinomial) based on the following common distance measures [18]: Euclidean (metric) distance, Cauchy–Schwarz (CS) divergence, Hellinger (metric) distance, Fisher-Rao (metric) distance, KL divergence and Hilbert simplicial (metric) distance. The Euclidean and Cauchy–Schwarz divergence are clipped to Δ^2 . The Cauchy–Schwarz distance is projective so that $\rho_{CS}(\lambda p, \lambda' q) = \rho_{CS}(p, q)$ for any $\lambda, \lambda' > 0$ [44].

4 Center-Based Clustering

We concentrate on comparing the efficiency of Hilbert simplex geometry for clustering multinomials. We shall compare the experimental results of k -means++ and k -center multinomial clustering for the three distances: Rao and Hilbert metric distances, and KL divergence. We describe how to adapt those clustering algorithms to the Hilbert distance.

4.1 k -means++ Clustering

The celebrated k -means clustering [45] minimizes the sum of within-cluster variances, where each cluster has a center representative element. When dealing with $k = 1$ cluster, the center (also called centroid or cluster prototype) is the center of mass defined as the minimizer of

$$E_D(\Lambda, c) = \frac{1}{n} \sum_{i=1}^n D(p_i : c),$$

where $D(\cdot : \cdot)$ is a dissimilarity measure. For an arbitrary D , the centroid c may not be available in closed form. Nevertheless, using a generalization of the k -means++ initialization [9] (picking randomly seeds), one can bypass the centroid computation, and yet guarantee probabilistically a good clustering.

Let $C = \{c_1, \dots, c_k\}$ denote the set of k cluster centers. Then the generalized k -means energy to be minimized is defined by:

$$E_D(\Lambda, C) = \frac{1}{n} \sum_{i=1}^n \min_{j \in \{1, \dots, k\}} D(p_i : c_j).$$

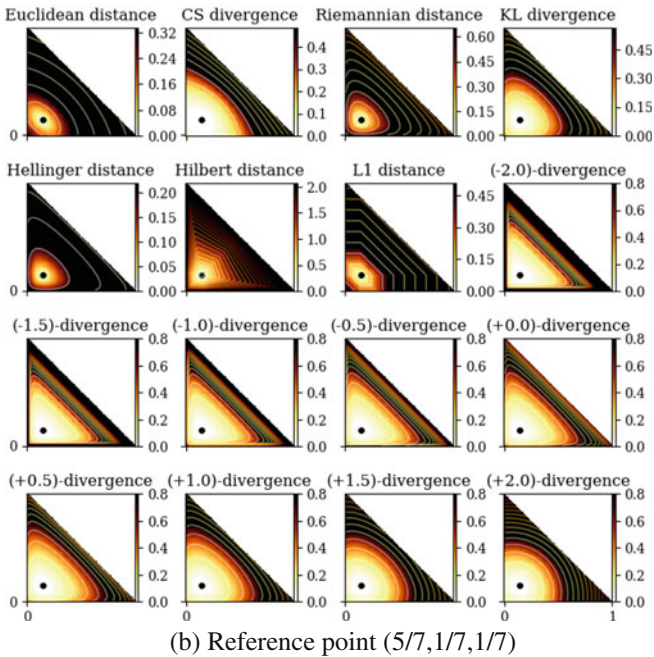
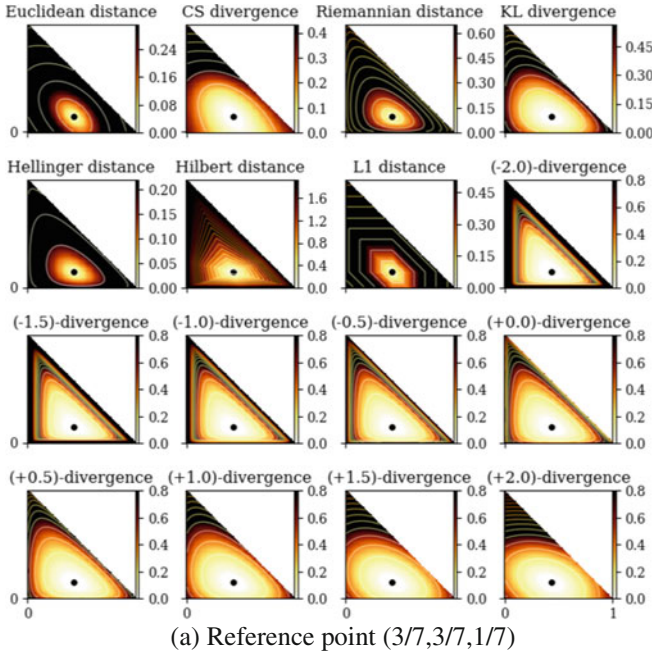


Fig. 7 A comparison of different distance measures on Δ^2 . The distance is measured from $\forall p \in \Delta^2$ to a fixed reference point (the black dot). Lighter color means shorter distance. Darker color means longer distance. The contours show equal distance curves with a precision step of 0.2

By defining the distance $D(p, C) = \min_{j \in \{1, \dots, k\}} D(p : c_j)$ of a point to a set, we can rewrite the objective function as $E_D(\Lambda, C) = \frac{1}{n} \sum_{i=1}^n D(p_i, C)$. Let $E_D^*(\Lambda, k) = \min_{C : |C|=k} E_D(\Lambda, C)$ denote the global minimum of $E_D(\Lambda, C)$ wrt some given Λ and k .

The k -means++ seeding proceeds for an arbitrary divergence D as follows: Pick uniformly at random at first seed c_1 , and then iteratively choose the $(k - 1)$ remaining seeds according to the following probability distribution:

$$\Pr(c_j = p_i) = \frac{D(p_i, \{c_1, \dots, c_{j-1}\})}{\sum_{i=1}^n D(p_i, \{c_1, \dots, c_{j-1}\})} \quad (2 \leq j \leq k).$$

Since its inception (2007), this k -means++ seeding has been extensively studied [46]. We state the general theorem established by [47]:

Theorem 2 (Generalized k -means++ performance, [47]) *Let κ_1 and κ_2 be two constants such that κ_1 defines the quasi-triangular inequality property:*

$$D(x : z) \leq \kappa_1 (D(x : y) + D(y : z)), \quad \forall x, y, z \in \Delta^d,$$

and κ_2 handles the symmetry inequality:

$$D(x : y) \leq \kappa_2 D(y : x), \quad \forall x, y \in \Delta^d.$$

Then the generalized k -means++ seeding guarantees with high probability a configuration C of cluster centers such that:

$$E_D(\Lambda, C) \leq 2\kappa_1^2 (1 + \kappa_2)(2 + \log k) E_D^*(\Lambda, k). \tag{7}$$

The ratio $\frac{E_D(\Lambda, C)}{E_D^*(\Lambda, k)}$ is called the *competitive factor*. The seminal result of ordinary k -means++ was shown [9] to be $8(2 + \log k)$ -competitive. When evaluating κ_1 , one has to note that squared metric distances are not metric because they do not satisfy the triangular inequality. For example, the squared Euclidean distance is not a metric but it satisfies the 2-quasi-triangular inequality with $\kappa_1 = 2$.

We state the following general performance theorem:

Theorem 3 (k -means++ performance in a metric space) *In any metric space (\mathcal{X}, d) , the k -means++ wrt the squared metric distance d^2 is $16(2 + \log k)$ -competitive.*

Proof Since a metric distance is symmetric, it follows that $\kappa_2 = 1$. Consider the quasi-triangular inequality property for the squared non-metric dissimilarity d^2 :

$$\begin{aligned} d(p, q) &\leq d(p, q) + d(q, r), \\ d^2(p, q) &\leq (d(p, q) + d(q, r))^2, \\ d^2(p, q) &\leq d^2(p, q) + d^2(q, r) + 2d(p, q)d(q, r). \end{aligned}$$

Let us apply the inequality of arithmetic and geometric means²:

$$\sqrt{d^2(p, q)d^2(q, r)} \leq \frac{d^2(p, q) + d^2(q, r)}{2}.$$

Thus we have

$$d^2(p, q) \leq d^2(p, q) + d^2(q, r) + 2d(p, q)d(q, r) \leq 2(d^2(p, q) + d^2(q, r)).$$

That is, the squared metric distance satisfies the 2-approximate triangle inequality, and $\kappa_1 = 2$. The result is straightforward from Theorem 2.

Theorem 4 (*k*-means++ performance in a normed space) *In any normed space $(\mathcal{X}, \|\cdot\|)$, the *k*-means++ with $D(x : y) = \|x - y\|^2$ is $16(2 + \log k)$ -competitive.*

Proof In any normed space $(\mathcal{X}, \|\cdot\|)$, we have both $\|x - y\| = \|y - x\|$ and the triangle inequality:

$$\|x - z\| \leq \|x - y\| + \|y - z\|.$$

The proof is very similar to the proof of Theorem 3 and is omitted.

Since any inner product space $(\mathcal{X}, \langle \cdot, \cdot \rangle)$ has an induced norm $\|x\| = \sqrt{\langle x, x \rangle}$, we have the following corollary.

Corollary 1 *In any inner product space $(\mathcal{X}, \langle \cdot, \cdot \rangle)$, the *k*-means++ with $D(x : y) = \langle x - y, x - y \rangle$ is $16(2 + \log k)$ -competitive.*

We need to report a bound for the squared Hilbert symmetric distance ($\kappa_2 = 1$). In [26] (Theorem 3.3), it was shown that Hilbert geometry of a bounded convex domain \mathcal{C} is isometric to a normed vector space iff \mathcal{C} is an open simplex: $(\Delta^d, \rho_{\text{HG}}) \simeq (V^d, \|\cdot\|_{\text{NH}})$, where $\|\cdot\|_{\text{NH}}$ is the corresponding norm. Therefore $\kappa_1 = 2$. We write “NH” for short for this equivalent normed Hilbert geometry. Appendix 8 recalls the construction due to [25], and shows the squared Hilbert distance fails the triangle inequality and it is not a distance induced by an inner product.

As an empirical study, we randomly generate $n = 10^6$ tuples (x, y, z) based on the uniform distribution in Δ^d . For each tuple (x, y, z) , we evaluate the ratio

$$\kappa_1 = \frac{D(x : z)}{D(x : y) + D(y : z)}.$$

Figure 8 shows the statistics for four different choices of D : (1) $D(x : y) = \rho_{\text{FHR}}^2(x, y)$; (2) $D(x : y) = \frac{1}{2}\text{KL}(x : y) + \frac{1}{2}\text{KL}(y : x)$; (3) $D(x : y) = \rho_{\text{HG}}^2(x, y)$; (4) $D(x : y) = \rho_{\text{L1}}^2(x, y)$. We find experimentally that κ_1 is upper bounded by 2 for ρ_{FHR}^2 , ρ_{HG}^2 and ρ_{L1}^2 , while the average κ_1 value is smaller than 0.5. For all the compared distances, $\kappa_2 = 1$. Therefore ρ_{FHR} and ρ_{HG} have better *k*-means++ performance guarantee as compared to ρ_{IG} .

²For positive values a and b , the arithmetic-geometric mean inequality states that $\sqrt{ab} \leq \frac{a+b}{2}$.

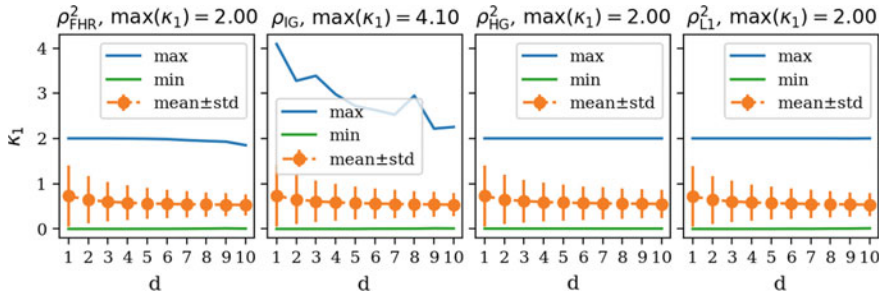


Fig. 8 The maximum, mean, standard deviation, and minimum of κ_1 on 10^6 randomly generated tuples (x, y, z) in Δ^d for $d = 1, \dots, 10$

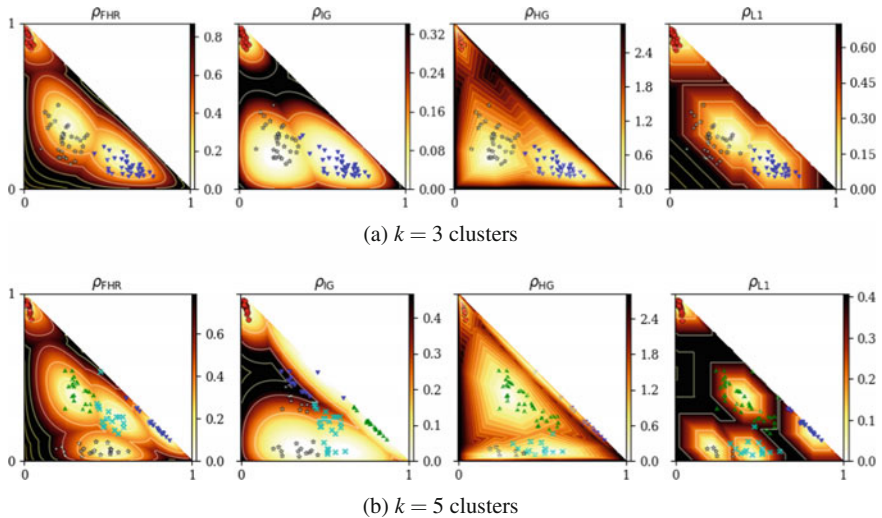


Fig. 9 k -Means++ clustering results on a toy dataset in the space of trinomials Δ^2 . The color density maps indicate the distance from any point to its nearest cluster center

We get by applying Theorem 4:

Corollary 2 (k -means++ in Hilbert simplex geometry) *The k -means++ seeding in a Hilbert simplex geometry in fixed dimension is $16(2 + \log k)$ -competitive.*

Figure 9 displays the clustering results of k -means++ in Hilbert simplex geometry as compared to the other geometries for $k \in \{3, 5\}$.

The KL divergence can be interpreted as a separable Bregman divergence [48]. The Bregman k -means++ performance has been studied in [48, 49], and a competitive factor of $O(\frac{1}{\mu})$ is reported using the notion of Bregman μ -similarity (that is suited for data-sets on a compact domain).

In [50], spherical k -means++ is studied wrt the distance $d_S(x, y) = 1 - \langle x, y \rangle$ for any pair of points x, y on the unit sphere. Since $\langle x, y \rangle = \|x\|_2 \|y\|_2 \cos(\theta_{x,y}) =$

$\cos(\theta_{x,y})$, we have $d_S(x, y) = 1 - \cos(\theta_{x,y})$, where $\theta_{x,y}$ denotes the angle between a pair of unit vectors x and y . This distance is called the cosine distance since it amounts to one minus the cosine similarity. Notice that the cosine distance is related to the squared Euclidean distance via the identity: $d_S(x, y) = \frac{1}{2}\|x - y\|^2$. The cosine distance is different from the spherical distance that relies on the arccos function.

Since divergences may be asymmetric, one can further consider mixed divergence $M(p : q : r) = \lambda D(p : q) + (1 - \lambda)D(q : r)$ for $\lambda \in [0, 1]$, and extend the k -means++ seeding procedure and analysis [51].

For a given data set, we can compute κ_1 or κ_2 by inspecting triples and pairs of points, and get data-dependent competitive factor improving the bounds mentioned above.

4.2 *k*-Center Clustering

Let Λ be a finite point set. The cost function for a k -center clustering with centers C ($|C| = k$) is:

$$f_D(\Lambda, C) = \max_{p_i \in \Lambda} \min_{c_j \in C} D(p_i : c_j).$$

The farthest first traversal heuristic [10] has a guaranteed approximation factor of 2 for any metric distance (see Algorithm 3).

In order to use the k -center clustering algorithm described in Algorithm 2, we need to be able to compute the 1-center (or minimax center) for the Hilbert simplex geometry, that is the Minimum Enclosing Ball (MEB, also called the Smallest Enclosing Ball, SEB).

Algorithm 2: k -Center clustering

Data: A set of points $p_1, \dots, p_n \in \Delta^d$. A distance measure ρ on Δ^d . The maximum number k of clusters. The maximum number T of iterations.

Result: A clustering scheme assigning each p_i a label $l_i \in \{1, \dots, k\}$

```

1 begin
2   Randomly pick  $k$  cluster centers  $c_1, \dots, c_k$  using the kmeans++ heuristic;
3   for  $t = 1, \dots, T$  do
4     for  $i = 1, \dots, n$  do
5        $l_i \leftarrow \arg \min_{l=1}^k \rho(p_i, c_l)$ ;
6     for  $l = 1, \dots, k$  do
7        $c_l \leftarrow \arg \min_c \max_{i:l_i=l} \rho(p_i, c)$ ;
8   Output  $\{l_i\}_{i=1}^n$ ;

```

Algorithm 3: A 2-approximation of the k -center clustering for any metric distance ρ .

Data: A set Λ ; a number k of clusters; a metric distance ρ .

Result: A 2-approximation of the k -center clustering

```

1 begin
2    $c_1 \leftarrow \text{ARandomPointOf}(\Lambda)$ ;
3    $C \leftarrow \{c_1\}$ ;
4   for  $i = 2, \dots, k$  do
5      $c_i \leftarrow \arg \max_{p \in \Lambda} \rho(p, C)$ ;
6      $C \leftarrow C \cup \{c_i\}$ ;
7 Output  $C$ ;
```

We may consider the SEB equivalently either in Δ^d or in the normed space V^d . In both spaces, the shapes of the balls are convex. Let $\Lambda = \{p_1, \dots, p_n\}$ denote the point set in Δ^d , and $\mathcal{V} = \{v_1, \dots, v_n\}$ the equivalent point set in the normed vector space (following the mapping explained in Appendix 8). Then the SEBs $B_{\text{HG}}(\Lambda)$ in Δ^d and $B_{\text{NH}}(\mathcal{V})$ in V^d have respectively radii r_{HG}^* and r_{NH}^* defined by:

$$r_{\text{HG}}^* = \min_{c \in \Delta^d} \max_{i \in \{1, \dots, n\}} \rho_{\text{HG}}(p_i, c),$$

$$r_{\text{NH}}^* = \min_{v \in V^d} \max_{i \in \{1, \dots, n\}} \|v_i - v\|_{\text{NH}}.$$

The SEB in the normed vector space $(V^d, \|\cdot\|_{\text{NH}})$ amounts to find the minimum covering norm polytope of a finite point set. This problem has been well-studied in computational geometry [52–54]. By considering the equivalent Hilbert norm polytope with $d(d+1)$ facets, we state the result of [54]:

Theorem 5 (SEB in Hilbert polytope normed space, [54]) *A $(1 + \varepsilon)$ -approximation of the SEB in V^d can be computed in $O(d^3 \frac{n}{\varepsilon})$ time.*

We shall now report two algorithms for computing the SEBs: One exact algorithm in V^d that does not scale well in high dimensions, and one approximation in Δ^d that works well for large dimensions.

4.2.1 Exact Smallest Enclosing Ball in a Hilbert Simplex Geometry

Given a finite point set $\{p_1, \dots, p_n\} \in \Delta^d$, the SEB in Hilbert simplex geometry is centered at

$$c^* = \arg \min_{c \in \Delta^d} \max_{i \in \{1, \dots, n\}} \rho_{\text{HG}}(c, x_i),$$

with radius

$$r^* = \min_{c \in \Delta^d} \max_{i \in \{1, \dots, n\}} \rho_{\text{HG}}(c, x_i).$$

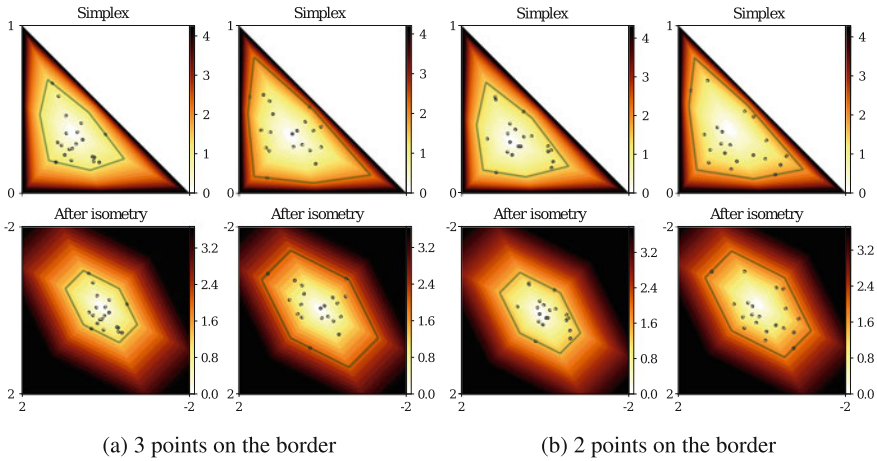


Fig. 10 Computing the SEB in Hilbert simplex geometry amounts to compute the SEB in the corresponding normed vector space

An equivalent problem is to find the SEB in the isometric normed vector space V^d via the mapping reported in Appendix 8. Each simplex point p_i corresponds to a point v_i in the V^d .

Figure 10 displays some examples of the exact smallest enclosing balls in the Hilbert simplex geometry and in the corresponding normed vector space.

To compute the SEB, one may also consider the generic LP-type randomized algorithm [55]. We notice that an enclosing ball for a point set in general has a number k of points on the border of the ball, with $2 \leq k \leq \frac{d(d+1)}{2}$. Let $D = \frac{d(d+1)}{2}$ denote the varying size of the combinatorial basis, then we can apply the LP-type framework (we check the axioms of locality and monotonicity, [56]) to solve efficiently the SEBs.

Theorem 6 (Smallest Enclosing Hilbert Ball is LP-type, [56, 57]) *The smallest enclosing Hilbert ball amounts to find the smallest enclosing ball in a vector space with respect to a polytope norm that can be solved using a LP-type randomized algorithm.*

The Enclosing Ball Decision Problem (EBDP, [58]) asks for a given value r , whether $r \geq r^*$ or not. The decision problem amounts to find whether a set $\{rB_V + v_i\}$ of translates can be stabbed by a point [58]: That is, whether $\cap_{i=1}^n (rB_V + v_i)$ is empty or not. Since these translates are polytopes with $d(d + 1)$ facets, this can be solved in linear time using *Linear Programming*.

Theorem 7 (Enclosing Hilbert Ball Decision Problem) *The decision problem to test whether $r \geq r^*$ or not can be solved by Linear Programming.*

This yields a simple scheme to approximate the optimal value r^* : Let $r_0 = \max_{i \in \{2, \dots, n\}} \|v_i - v_1\|_{\text{NH}}$. Then $r^* \in [\frac{r_0}{2}, r_0] = [a_0, b_0]$. At stage i , perform a dichotomic search on $[a_i, b_i]$ by answering the decision problem for $r_{i+1} = \frac{a_i + b_i}{2}$, and update the radius range accordingly [58].

However, the LP-type randomized algorithm or the decision problem-based algorithm do not scale well in high dimensions. Next, we introduce a simple approximation algorithm that relies on the fact that the line segment $[pq]$ is a geodesic in Hilbert simplex geometry. (Geodesics are not unique. See Figure 2 of [25].)

4.2.2 Geodesic Bisection Approximation Heuristic

In Riemannian geometry, the 1-center can be arbitrarily finely approximated by a simple geodesic bisection algorithm [59, 60]. This algorithm can be extended to HG straightforwardly as detailed in Algorithm 4.

Algorithm 4: Geodesic walk for approximating the Hilbert minimax center, generalizing [60]

Data: A set of points $p_1, \dots, p_n \in \Delta^d$. The maximum number T of iterations.

Result: $c \approx \arg \min_c \max_i \rho_{\text{HG}}(p_i, c)$

```

1 begin
2    $c_0 \leftarrow \text{ARandomPointOf}(\{p_1, \dots, p_n\});$ 
3   for  $t = 1, \dots, T$  do
4      $p \leftarrow \arg \max_{p_i} \rho_{\text{HG}}(p_i, c_{t-1});$ 
5      $c_t \leftarrow c_{t-1} \#_{1/(t+1)}^\rho p;$ 
6   Output  $c_T;$ 

```

The algorithm first picks up a point c_0 at random from Λ as the initial center, then computes the farthest point p (with respect to the distance ρ), and then walk on the geodesic from c_0 to p by a certain amount to define c_1 , etc. For an arbitrary distance ρ , we define the operator $\#_\alpha^\rho$ as follows:

$$p \#_\alpha^\rho q = v = \gamma(p, q, \alpha), \quad \rho(p : v) = \alpha \rho(p : q),$$

where $\gamma(p, q, \alpha)$ is the geodesic passing through p and q , and parameterized by α ($0 \leq \alpha \leq 1$). When the equations of the geodesics are explicitly known, we can either get a closed form solution for $\#_\alpha^\rho$ or perform a bisection search to find v' such that $\rho(p : v') \approx \alpha \rho(p : q)$. See [61] for an extension and analysis in hyperbolic geometry. See Fig. 11 to get an intuitive idea on the *experimental* convergence rate of Algorithm 4. See Fig. 12 for visualizations of centers wrt different geometries.

Furthermore, this iterative algorithm implies a core-set [62] (namely, the set of farthest points visited during the geodesic walks) that is useful for clustering large

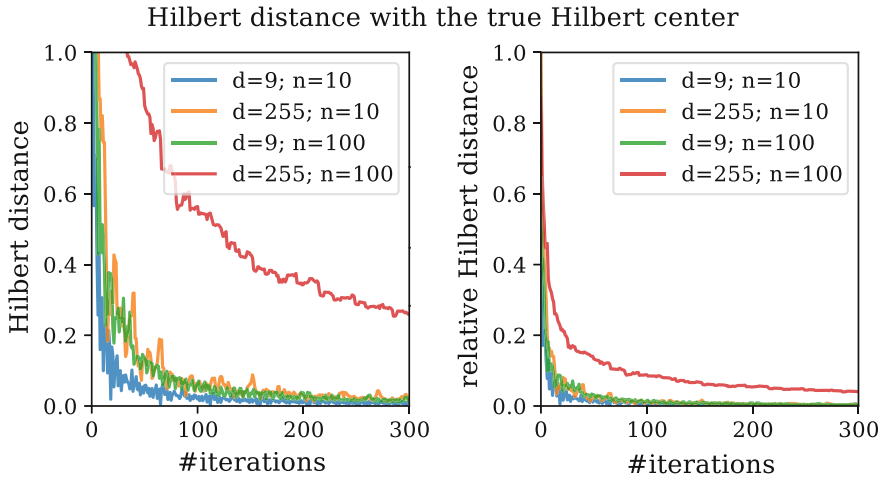


Fig. 11 Convergence rate of Algorithm 4 measured by the Hilbert distance between the current minimax center and the true center (left) or their Hilbert distance divided by the Hilbert radius of the dataset (right). The plot is based on 100 random points in Δ^9/Δ^{255}

data-sets [63]. See [52] for core-set results on containment problems wrt a convex homothetic object (the equivalent Hilbert polytope norm in our case).

A simple algorithm dubbed MINCON [53] can find an approximation of the Minimum Enclosing Polytope. The algorithm induces a core-set of size $O(\frac{1}{\epsilon^2})$ although the theorem is challenged in [52].

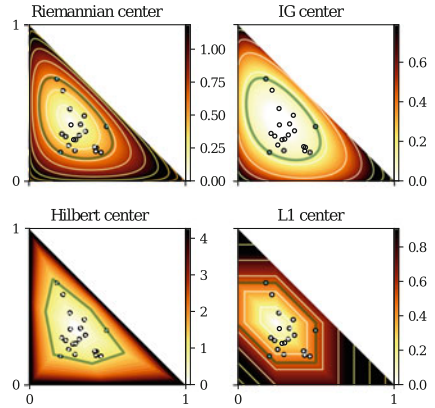
Thus by combining the k -center seeding [10] with the Lloyd-like batched iterations, we get an efficient k -center clustering algorithm for the FHR and Hilbert metric geometries. When dealing with the Kullback–Leibler divergence, we use the fact that KL is a Bregman divergence, and use the 1-center algorithm ([64, 65] for approximation in any dimension, or [55] which is exact but limited to small dimensions).

Since Hilbert simplex geometry is isomorphic to a normed vector space [26] with a polytope norm with $d(d+1)$ facets, the Voronoi diagram in Hilbert geometry of Δ^d amounts to compute a Voronoi diagram wrt a polytope norm [66–68].

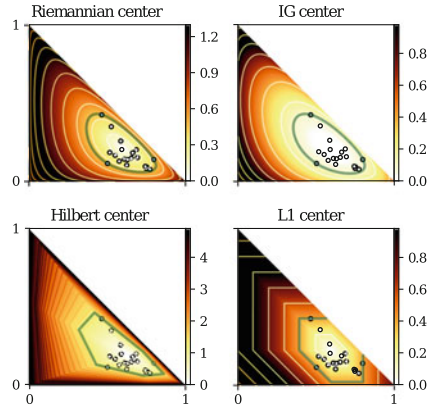
5 Experiments

We generate a dataset consisting of a set of clusters in a high dimensional statistical simplex Δ^d . Each cluster is generated independently as follows. We first pick a random center $c = (\lambda_c^0, \dots, \lambda_c^d)$ based on the uniform distribution on Δ^d . Then any random sample $p = (\lambda^0, \dots, \lambda^d)$ associated with c is independently generated by

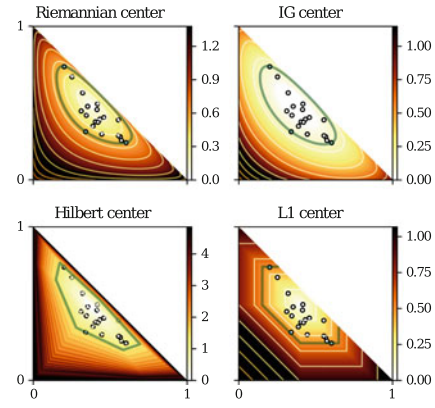
Fig. 12 The Riemannian/IG/Hilbert/ L_1 minimax centers of three point clouds in Δ^2 based on Algorithm 4. The color maps show the distance from $\forall p \in \Delta^2$ to the corresponding center



(a) Point Cloud 1



(b) Point Cloud 2



(c) Point Cloud 3

$$\lambda^i = \frac{\exp(\log \lambda_c^i + \sigma \varepsilon^i)}{\sum_{i=0}^d \exp(\log \lambda_c^i + \sigma \varepsilon^i)},$$

where $\sigma > 0$ is a noise level parameter, and each ε^i follows independently a standard Gaussian distribution (generator 1) or the Student's t -distribution with five degrees of freedom (generator 2). Let $\sigma = 0$, we get $\lambda^i = \lambda_c^i$. Therefore p is randomly distributed around c . We repeat generating random samples for each cluster center, and make sure that different clusters have almost the same number of samples. Then we perform clustering based on the configurations $n \in \{50, 100\}$, $d \in \{9, 255\}$, $\sigma \in \{0.5, 0.9\}$, $\rho \in \{\rho_{\text{FHR}}, \rho_{\text{IG}}, \rho_{\text{HG}}, \rho_{\text{EUC}}, \rho_{\text{LI}}\}$. For simplicity, the number of clusters k is set to the ground truth. For each configuration, we repeat the clustering experiment based on 300 different random datasets. The performance is measured by the normalized mutual information (NMI), which is a scalar indicator in the range $[0, 1]$ (the larger the better).

The results of k -means++ and k -centers are shown in Tables 2 and 3, respectively. The large variance of NMI is because that each experiment is performed on random datasets wrt different random seeds. Generally, the performance deteriorates as we increase the number of clusters, increase the noise level or decrease the dimensionality, which have the same effect to reduce the inter-cluster gap.

The key comparison is the three columns ρ_{FHR} , ρ_{HG} and ρ_{IG} , as they are based on exactly the same algorithm with the only difference being the underlying geometry. We see clearly that in general, their clustering performance presents the order $\text{HG} > \text{FHR} > \text{IG}$. The performance of HG is superior to the other two geometries, especially when the noise level is large. Intuitively, the Hilbert balls are more compact in size and therefore can better capture the clustering structure (see Fig. 2).

The column ρ_{EUC} is based on the Euclidean enclosing ball. It shows the worst scores because the intrinsic geometry of the probability simplex is far from the Euclidean geometry.

6 Hilbert's Projective Geometry of the Space of Correlation Matrices

In this section, we present the Hilbert's projective geometry to the space of correlation matrices

$$\mathcal{C}^d = \{C_{d \times d} : C > 0; C_{ii} = 1, \forall i\}.$$

If $C_1, C_2 \in \mathcal{C}$, then $(1 - \lambda)C_1 + \lambda C_2 \in \mathcal{C}$ for $0 < \lambda < 1$. Therefore \mathcal{C} is a convex set, known as an *elliptope* [11] embedded in the p.s.d. cone. See Fig. 13 for an intuitive view of \mathcal{C}_3 , where the coordinate system (x, y, z) is the off-diagonal entries of $C \in \mathcal{C}_3$.

In order to compute the Hilbert distance $\rho_{\text{HG}}(C_1, C_2)$, we need to compute the intersection of the line (C_1, C_2) with $\partial\mathcal{C}$, denoted as C'_1 and C'_2 , then we have

Table 2 k -means++ clustering accuracy in NMI on randomly generated datasets based on different geometries. The table shows the mean and standard deviation after 300 independent runs for each configuration. ρ is the distance measure. n is the sample size. d is the dimensionality of Δ^d . σ is noise level

k	n	d	σ	ρ_{FHR}	ρ_{IG}	ρ_{HG}	ρ_{EUC}	ρ_{L1}	
3	50	9	0.5	0.76 ± 0.22	0.76 ± 0.24	0.81 ± 0.22	0.64 ± 0.23	0.70 ± 0.22	
			0.9	0.44 ± 0.20	0.44 ± 0.20	0.57 ± 0.22	0.31 ± 0.17	0.38 ± 0.18	
		255	0.5	0.80 ± 0.24	0.81 ± 0.24	0.88 ± 0.21	0.74 ± 0.25	0.79 ± 0.24	
			0.9	0.65 ± 0.27	0.66 ± 0.28	0.72 ± 0.27	0.46 ± 0.24	0.63 ± 0.27	
		100	9	0.5	0.76 ± 0.22	0.76 ± 0.21	0.82 ± 0.22	0.60 ± 0.21	0.69 ± 0.23
				0.9	0.42 ± 0.19	0.41 ± 0.18	0.54 ± 0.22	0.27 ± 0.14	0.34 ± 0.16
	255		0.5	0.82 ± 0.23	0.82 ± 0.24	0.89 ± 0.20	0.74 ± 0.24	0.80 ± 0.25	
			0.9	0.66 ± 0.26	0.66 ± 0.28	0.72 ± 0.26	0.45 ± 0.25	0.64 ± 0.27	
	5	50	9	0.5	0.75 ± 0.14	0.74 ± 0.15	0.81 ± 0.13	0.61 ± 0.13	0.68 ± 0.13
				0.9	0.44 ± 0.13	0.42 ± 0.13	0.55 ± 0.15	0.31 ± 0.11	0.36 ± 0.12
			255	0.5	0.83 ± 0.15	0.83 ± 0.15	0.88 ± 0.14	0.77 ± 0.16	0.82 ± 0.15
				0.9	0.71 ± 0.17	0.70 ± 0.19	0.75 ± 0.17	0.50 ± 0.17	0.68 ± 0.18
100			9	0.5	0.74 ± 0.13	0.74 ± 0.14	0.80 ± 0.14	0.60 ± 0.13	0.67 ± 0.13
				0.9	0.42 ± 0.11	0.40 ± 0.12	0.55 ± 0.15	0.29 ± 0.09	0.35 ± 0.11
		255	0.5	0.83 ± 0.14	0.83 ± 0.15	0.88 ± 0.13	0.77 ± 0.15	0.81 ± 0.15	
			0.9	0.69 ± 0.18	0.69 ± 0.18	0.73 ± 0.17	0.48 ± 0.17	0.67 ± 0.18	

(a) Generator 1

k	n	d	σ	ρ_{FHR}	ρ_{IG}	ρ_{HG}	ρ_{EUC}	ρ_{L1}	
3	50	9	0.5	0.62 ± 0.22	0.60 ± 0.22	0.71 ± 0.23	0.45 ± 0.20	0.54 ± 0.22	
			0.9	0.29 ± 0.17	0.27 ± 0.16	0.39 ± 0.19	0.17 ± 0.13	0.25 ± 0.15	
		255	0.5	0.70 ± 0.25	0.69 ± 0.26	0.74 ± 0.25	0.37 ± 0.29	0.70 ± 0.26	
			0.9	0.42 ± 0.25	0.35 ± 0.20	0.40 ± 0.19	0.03 ± 0.08	0.44 ± 0.26	
		100	9	0.5	0.63 ± 0.22	0.61 ± 0.22	0.71 ± 0.22	0.46 ± 0.19	0.56 ± 0.20
				0.9	0.29 ± 0.15	0.26 ± 0.14	0.38 ± 0.20	0.18 ± 0.12	0.24 ± 0.14
	255		0.5	0.71 ± 0.26	0.69 ± 0.27	0.75 ± 0.25	0.31 ± 0.28	0.70 ± 0.27	
			0.9	0.41 ± 0.26	0.33 ± 0.20	0.38 ± 0.18	0.02 ± 0.06	0.43 ± 0.26	
	5	50	9	0.5	0.64 ± 0.15	0.61 ± 0.14	0.70 ± 0.14	0.48 ± 0.14	0.57 ± 0.15
				0.9	0.31 ± 0.12	0.29 ± 0.12	0.41 ± 0.15	0.20 ± 0.09	0.26 ± 0.10
			255	0.5	0.74 ± 0.17	0.72 ± 0.17	0.77 ± 0.16	0.41 ± 0.20	0.74 ± 0.17
				0.9	0.44 ± 0.17	0.37 ± 0.16	0.44 ± 0.15	0.04 ± 0.06	0.47 ± 0.17
100			9	0.5	0.62 ± 0.14	0.61 ± 0.14	0.71 ± 0.14	0.46 ± 0.13	0.54 ± 0.14
				0.9	0.30 ± 0.10	0.27 ± 0.11	0.40 ± 0.13	0.19 ± 0.08	0.25 ± 0.09
		255	0.5	0.73 ± 0.18	0.70 ± 0.18	0.75 ± 0.16	0.37 ± 0.20	0.73 ± 0.17	
			0.9	0.43 ± 0.16	0.35 ± 0.14	0.41 ± 0.12	0.03 ± 0.06	0.46 ± 0.18	

(b) Generator 2

Table 3 k -center clustering accuracy in NMI on randomly generated datasets based on different geometries. The table shows the mean and standard deviation after 300 independent runs for each configuration. ρ is the distance measure. n is the sample size. d is the dimensionality of the statistical simplex. σ is noise level

k	n	d	σ	ρ_{FHR}	ρ_{IG}	ρ_{HG}	ρ_{EUC}	ρ_{L1}
3	50	9	0.5	0.87 ± 0.19	0.85 ± 0.19	0.92 ± 0.16	0.72 ± 0.22	0.80 ± 0.20
			0.9	0.54 ± 0.21	0.51 ± 0.21	0.70 ± 0.23	0.36 ± 0.17	0.44 ± 0.19
		255	0.5	0.93 ± 0.16	0.92 ± 0.18	0.95 ± 0.14	0.89 ± 0.18	0.90 ± 0.19
			0.9	0.76 ± 0.24	0.72 ± 0.26	0.82 ± 0.24	0.50 ± 0.28	0.76 ± 0.25
	100	9	0.5	0.88 ± 0.17	0.86 ± 0.18	0.93 ± 0.14	0.70 ± 0.20	0.80 ± 0.20
			0.9	0.53 ± 0.20	0.49 ± 0.19	0.70 ± 0.22	0.33 ± 0.14	0.41 ± 0.18
		255	0.5	0.93 ± 0.16	0.92 ± 0.17	0.95 ± 0.13	0.88 ± 0.19	0.93 ± 0.16
			0.9	0.81 ± 0.22	0.75 ± 0.24	0.83 ± 0.22	0.47 ± 0.28	0.79 ± 0.22
5	50	9	0.5	0.82 ± 0.13	0.81 ± 0.13	0.89 ± 0.12	0.67 ± 0.13	0.75 ± 0.13
			0.9	0.50 ± 0.13	0.47 ± 0.13	0.66 ± 0.15	0.34 ± 0.11	0.40 ± 0.12
		255	0.5	0.92 ± 0.11	0.91 ± 0.12	0.93 ± 0.11	0.87 ± 0.13	0.92 ± 0.12
			0.9	0.77 ± 0.15	0.71 ± 0.17	0.85 ± 0.17	0.54 ± 0.19	0.74 ± 0.16
	100	9	0.5	0.83 ± 0.12	0.81 ± 0.13	0.89 ± 0.11	0.67 ± 0.11	0.76 ± 0.13
			0.9	0.48 ± 0.12	0.46 ± 0.12	0.66 ± 0.15	0.33 ± 0.09	0.39 ± 0.10
		255	0.5	0.93 ± 0.10	0.92 ± 0.11	0.94 ± 0.09	0.89 ± 0.11	0.92 ± 0.11
			0.9	0.81 ± 0.14	0.74 ± 0.15	0.84 ± 0.16	0.52 ± 0.19	0.79 ± 0.14

(a) Generator 1

k	n	d	σ	ρ_{FHR}	ρ_{IG}	ρ_{HG}	ρ_{EUC}	ρ_{L1}
3	50	9	0.5	0.68 ± 0.22	0.67 ± 0.22	0.80 ± 0.20	0.48 ± 0.22	0.60 ± 0.22
			0.9	0.32 ± 0.18	0.29 ± 0.17	0.45 ± 0.21	0.20 ± 0.14	0.26 ± 0.15
		255	0.5	0.79 ± 0.24	0.75 ± 0.24	0.82 ± 0.22	0.13 ± 0.23	0.81 ± 0.24
			0.9	0.35 ± 0.27	0.35 ± 0.21	0.42 ± 0.19	0.00 ± 0.02	0.32 ± 0.30
	100	9	0.5	0.66 ± 0.22	0.65 ± 0.22	0.79 ± 0.21	0.45 ± 0.19	0.59 ± 0.20
			0.9	0.30 ± 0.16	0.28 ± 0.14	0.42 ± 0.19	0.20 ± 0.12	0.26 ± 0.14
		255	0.5	0.78 ± 0.25	0.76 ± 0.24	0.82 ± 0.21	0.05 ± 0.14	0.77 ± 0.27
			0.9	0.29 ± 0.28	0.29 ± 0.20	0.39 ± 0.20	0.00 ± 0.02	0.22 ± 0.25
5	50	9	0.5	0.69 ± 0.14	0.66 ± 0.14	0.77 ± 0.13	0.50 ± 0.13	0.61 ± 0.14
			0.9	0.34 ± 0.12	0.30 ± 0.12	0.46 ± 0.15	0.22 ± 0.09	0.28 ± 0.10
		255	0.5	0.80 ± 0.15	0.76 ± 0.15	0.82 ± 0.14	0.24 ± 0.23	0.81 ± 0.14
			0.9	0.42 ± 0.21	0.38 ± 0.16	0.46 ± 0.15	0.00 ± 0.02	0.39 ± 0.22
	100	9	0.5	0.66 ± 0.13	0.64 ± 0.14	0.77 ± 0.14	0.47 ± 0.13	0.57 ± 0.13
			0.9	0.31 ± 0.11	0.28 ± 0.10	0.44 ± 0.13	0.21 ± 0.08	0.25 ± 0.09
		255	0.5	0.80 ± 0.16	0.76 ± 0.15	0.82 ± 0.13	0.12 ± 0.17	0.81 ± 0.16
			0.9	0.32 ± 0.19	0.30 ± 0.15	0.41 ± 0.13	0.00 ± 0.01	0.26 ± 0.18

(b) Generator 2

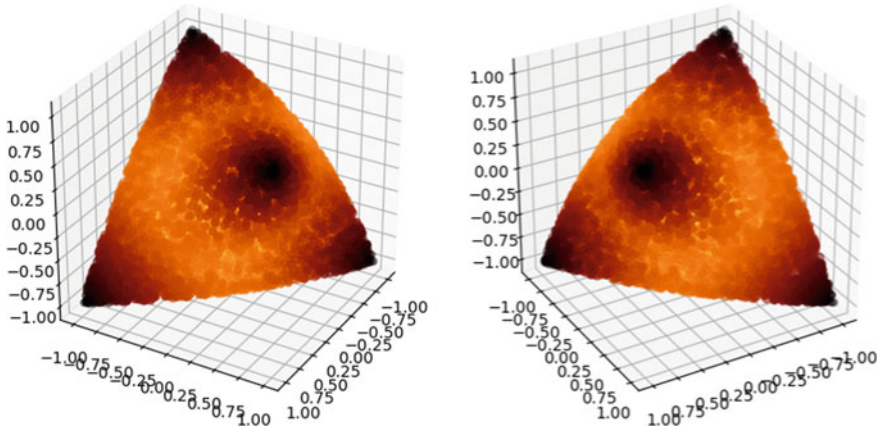


Fig. 13 The elliptope \mathcal{E}_3 (two different perspectives)

$$\rho_{HG}(C_1, C_2) = \left| \log \frac{\|C_1 - C_2\| \|C'_1 - C_2\|}{\|C_1 - C'_1\| \|C_2 - C'_2\|} \right|.$$

Unfortunately there is no closed form solution of C'_1 and C'_2 . Instead, we apply a binary searching algorithm. Note a necessary condition for $C \in \mathcal{E}$ is that C has a positive spectrum. If C has at least one non-positive eigenvalue, then $C \notin \mathcal{E}$. To determine whether a given C is inside the elliptope requires a spectral decomposition of C . Therefore the computation of C'_1 and C'_2 is in general expensive.

We compare the Hilbert elliptope geometry with commonly used distance measures including the L_2 distance ρ_{EUC} , L_1 distance ρ_{L1} , and the square root of the log-det divergence

$$\rho_{LD}(C_1, C_2) = \text{tr}(C_1 C_2^{-1}) - \log |C_1 C_2^{-1}| - d.$$

Due to the high computational complexity, we only investigate k -means++ clustering. The investigated dataset consists of 100 matrices forming 3 clusters in \mathcal{E}_3 with almost identical size. Each cluster is independently generated according to

$$\begin{aligned} P &\sim \mathcal{W}^{-1}(I_{3 \times 3}, \nu_1), \\ C_i &\sim \mathcal{W}^{-1}(P, \nu_2), \end{aligned}$$

where $\mathcal{W}^{-1}(A, \nu)$ denotes the inverse Wishart distribution with scale matrix A and ν degrees of freedom, and C_i is a point in the cluster associated with P . Table 4 shows the k -means++ clustering performance in terms of NMI. Again Hilbert geometry is favorable as compared to alternatives, showing that the good performance of Hilbert clustering is generalizable.

Table 4 NMI (mean \pm std) of k -means++ clustering based on different distance measures in the elliptope (500 independent runs)

ν_1	ν_2	ρ_{HG}	ρ_{EUC}	ρ_{L1}	ρ_{LD}
4	10	0.62 \pm 0.22	0.57 \pm 0.21	0.56 \pm 0.22	0.58 \pm 0.22
4	30	0.85 \pm 0.18	0.80 \pm 0.20	0.81 \pm 0.19	0.82 \pm 0.20
4	50	0.89 \pm 0.17	0.87 \pm 0.17	0.86 \pm 0.18	0.88 \pm 0.18
5	10	0.50 \pm 0.21	0.49 \pm 0.21	0.48 \pm 0.20	0.47 \pm 0.21
5	30	0.77 \pm 0.20	0.75 \pm 0.21	0.75 \pm 0.21	0.75 \pm 0.21
5	50	0.84 \pm 0.19	0.82 \pm 0.19	0.82 \pm 0.20	0.84 \pm 0.18

7 Conclusion

We introduced the Hilbert projective metric distance and its underlying non-Riemannian geometry for modeling the space of multinomials or the open probability simplex. We compared experimentally in simulated clustering tasks this geometry with the traditional differential geometric modelings (either the Fisher-Hotelling-Rao metric connection or the dually coupled non-metric affine connections of information geometry [17]).

The main feature of Hilbert geometry (HG) is that it is a metric non-manifold geometry, where geodesics are straight (Euclidean) line segments. This makes this geometry computationally attractive. In simplex domains, the Hilbert balls have fixed combinatorial (Euclidean) polytope structures, and HG is known to be isometric to a normed space [25, 69]. This latter isometry allows one to generalize easily the standard proofs of clustering (e.g., k -means or k -center). We demonstrated it for the k -means++ competitive performance analysis and for the convergence of the 1-center heuristic [60] (smallest enclosing Hilbert ball allows one to implement efficiently the k -center clustering). Our experimental k -means++ or k -center comparisons of HG algorithms with the manifold modeling approach yield superior performance. This may be intuitively explained by the sharpness of Hilbert balls as compared to the FHR/IG ball profiles.

Chentsov [70] defined statistical invariance on a probability manifold under Markov morphisms and proved that the Fisher Information Metric is the unique Riemannian metric (up to rescaling) for multinomials. However, this does not rule out that other distances (with underlying geometric structures) may be used to model statistical manifolds (e.g., Finsler statistical manifolds [71, 72], or the total variation distance — the only metric f -divergence [73]). Defining statistical invariance related to geometry is the cornerstone problem of information geometry that can be tackled from many directions (see [74] and references therein for a short review).

In this paper, we introduced Hilbert geometries in machine learning by considering clustering tasks in the probability simplex and in the correlation elliptope. A canonical Hilbert metric distance can be defined on any bounded convex subset of the Euclidean space with the key property that geodesics are straight Euclidean line segments thus

making this geometry well-suited for fast and exact computations. Thus we may consider clustering in other bounded convex subsets like the simplotopes [75].

One future direction is to consider the Hilbert metric for regularization and sparsity in machine learning (due to its equivalence with a polytope normed distance).

Our Python codes are freely available online for reproducible research:

<https://www.lix.polytechnique.fr/~nielsen/HSG/>

8 Isometry of Hilbert Simplex Geometry to a Normed Vector Space

Consider the Hilbert simplex metric space (Δ^d, ρ_{HG}) where Δ^d denotes the d -dimensional open probability simplex and ρ_{HG} the Hilbert cross-ratio metric. Let us recall the isometry ([25], 1991) of the open standard simplex to a normed vector space $(V^d, \|\cdot\|_{NH})$. Let $V^d = \{v \in \mathbb{R}^{d+1} : \sum_i v^i = 0\}$ denote the d -dimensional vector space sitting in \mathbb{R}^{d+1} . Map a point $p = (\lambda^0, \dots, \lambda^d) \in \Delta^d$ to a point $v(x) = (v^0, \dots, v^d) \in V^d$ as follows:

$$v^i = \frac{1}{d+1} \left(d \log \lambda^i - \sum_{j \neq i} \log \lambda^j \right) = \log \lambda^i - \frac{1}{d+1} \sum_j \log \lambda^j.$$

We define the corresponding norm $\|\cdot\|_{NH}$ in V^d by considering the shape of its unit ball $B_V = \{v \in V^d : |v^i - v^j| \leq 1, \forall i \neq j\}$. The unit ball B_V is a symmetric convex set containing the origin in its interior, and thus yields a *polytope norm* $\|\cdot\|_{NH}$ (Hilbert norm) with $2\binom{d+1}{2} = d(d+1)$ facets. Reciprocally, let us notice that a norm induces a unit ball centered at the origin that is convex and symmetric around the origin.

The distance in the normed vector space between $v \in V^d$ and $v' \in V^d$ is defined by:

$$\rho_V(v, v') = \|v - v'\|_{NH} = \inf \{ \tau : v' \in \tau(B_V \oplus \{v\}) \},$$

where $A \oplus B = \{a + b : a \in A, b \in B\}$ is the Minkowski sum.

The reverse map from the normed space V^d to the probability simplex Δ^d is given by:

$$\lambda^i = \frac{\exp(v^i)}{\sum_j \exp(v^j)}.$$

Thus we have $(\Delta^d, \rho_{HG}) \cong (V^d, \|\cdot\|_{NH})$. In 1D, $(V^1, \|\cdot\|_{NH})$ is isometric to the Euclidean line.

Note that computing the distance in the normed vector space requires naively $O(d^2)$ time.

Unfortunately, the norm $\| \cdot \|_{\text{NH}}$ does not satisfy the parallelogram law.³ Notice that a norm satisfying the parallelogram law can be associated with an inner product via the polarization identity. Thus the isometry of the Hilbert geometry to a normed vector space is not equipped with an inner product. However, all norms in a finite dimensional space are equivalent. This implies that in finite dimension, $(\Delta^d, \rho_{\text{HG}})$ is *quasi-isometric* to the Euclidean space \mathbb{R}^d . An example of Hilbert geometry in infinite dimension is reported in [25]. Hilbert spaces are not CAT spaces except when \mathcal{C} is an ellipsoid [76].

9 Hilbert Geometry with Finslerian/Riemannian Structures

In a Riemannian geometry, each tangent plane T_pM of a d -dimensional manifold M is equivalent to \mathbb{R}^d : $T_pM \simeq \mathbb{R}^d$. The inner product at each tangent plane T_pM can be visualized by an ellipsoid shape, a convex symmetric object centered at point p . In a *Finslerian geometry*, a norm $\| \cdot \|_p$ is defined in each tangent plane T_pM , and this norm is visualized as a symmetric convex object with non-empty interior. Finslerian geometry thus generalizes Riemannian geometry by taking into account generic symmetric convex objects instead of ellipsoids for inducing norms at each tangent plane. Any Hilbert geometry induced by a compact convex domain \mathcal{C} can be expressed by an equivalent Finslerian geometry by defining the norm in T_p at p as follows [76]:

$$\|v\|_p = F_{\mathcal{C}}(p, v) = \frac{\|v\|}{2} \left(\frac{1}{pp^+} + \frac{1}{pp^-} \right),$$

where $F_{\mathcal{C}}$ is the *Finsler metric*, $\| \cdot \|$ is an *arbitrary norm* on \mathbb{R}^d , and p^+ and p^- are the intersection points of the line passing through p with direction v :

$$p^+ = p + t^+v, \quad p^- = p + t^-v.$$

A geodesic γ in a Finslerian geometry satisfies:

$$d_{\mathcal{C}}(\gamma(t_1), \gamma(t_2)) = \int_{t_1}^{t_2} F_{\mathcal{C}}(\gamma(t), \dot{\gamma}(t))dt.$$

In T_pM , a ball of center c and radius r is defined by:

$$B(c, r) = \{v : F_{\mathcal{C}}(c, v) \leq r\}.$$

³Consider $A = (1/3, 1/3, 1/3)$, $B = (1/6, 1/2, 1/3)$, $C = (1/6, 2/3, 1/6)$ and $D = (1/3, 1/2, 1/6)$. Then $2AB^2 + 2BC^2 = 4.34$ but $AC^2 + BD^2 = 3.84362411135$.

Thus any Hilbert geometry induces an equivalent Finslerian geometry, and since Finslerian geometries include Riemannian geometries, one may wonder which Hilbert geometries induce Riemannian structures? The only Riemannian geometries induced by Hilbert geometries are the *hyperbolic Cayley–Klein geometries* [27, 29, 30] with the domain \mathcal{C} being an ellipsoid. The Finslerian modeling of information geometry has been studied in [71, 72].

There is not a canonical way of defining measures in a Hilbert geometry since Hilbert geometries are Finslerian but not necessary Riemannian geometries [76]. The Busemann measure is defined according to the Lebesgue measure λ of \mathbb{R}^d : Let B_p denote the unit ball wrt. to the Finsler norm at point $p \in \mathcal{C}$, and B_e the Euclidean unit ball. Then the Busemann measure for a Borel set \mathcal{B} is defined by [76]:

$$\mu_{\mathcal{C}}(\mathcal{B}) = \int_{\mathcal{B}} \frac{\lambda(B_e)}{\lambda(B_p)} d\lambda(p).$$

The existence and uniqueness of center points of a probability measure in Finsler geometry have been investigated in [77].

10 Bounding Hilbert Norm with Other Norms

Let us show that $\|v\|_{\text{NH}} \leq \beta_{d,c} \|v\|_c$, where $\|\cdot\|_c$ is any norm. Let $v = \sum_{i=0}^d e_i x_i$, where $\{e_i\}$ is a basis of \mathbb{R}^{d+1} . We have:

$$\|v\|_c \leq \sum_{i=0}^d |x_i| \|e_i\|_c \leq \|x\|_2 \underbrace{\sqrt{\sum_{i=0}^d \|e_i\|_c^2}}_{\beta_d},$$

where the first inequality comes from the triangle inequality, and the second inequality is from the Cauchy–Schwarz inequality. Thus we have:

$$\|v\|_{\text{NH}} \leq \beta_d \|x\|_2,$$

with $\beta_d = \sqrt{d+1}$ since $\|e_i\|_{\text{NH}} \leq 1$.

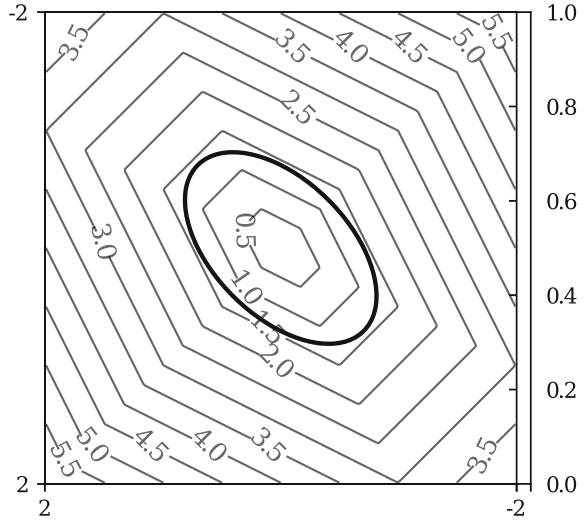
Let $\alpha_{d,c} = \min_{\{v : \|v\|_c=1\}} \|v\|_{\text{NH}}$. Consider $u = \frac{v}{\|v\|_c}$. Then $\|u\|_c = 1$ so that $\|v\|_{\text{NH}} \geq \alpha_{d,c} \|v\|_c$. To find α_d , we consider the unit ℓ_2 ball in V^d , and find the smallest $\lambda > 0$ so that λB_V fully contains the Euclidean ball (Fig. 14).

Therefore, we have overall:

$$\alpha_d \|x\|_2 \leq \|v\|_{\text{NH}} \leq \sqrt{d+1} \|x\|_2$$

In general, note that we may consider two arbitrary norms $\|\cdot\|_l$ and $\|\cdot\|_u$ so that:

Fig. 14 Polytope balls B_V and the Euclidean unit ball B_E . From the figure the smallest polytope ball has radius ≈ 1.5



$$\alpha_{d,l} \|x\|_l \leq \|v\|_{NH} \leq \beta_{d,u} \|x\|_u.$$

11 Funk Directed Metrics and Funk Balls

The Funk metric [78] wrt a convex domain \mathcal{C} is defined by

$$F_{\mathcal{C}}(x, y) = \log \left(\frac{\|x - a\|}{\|y - a\|} \right),$$

where a is the intersection of the domain boundary and the affine ray $R(x, y)$ starting from x and passing through y . Correspondingly, the reverse Funk metric is

$$F_{\mathcal{C}}(y, x) = \log \left(\frac{\|y - b\|}{\|x - b\|} \right),$$

where b is the intersection of $R(y, x)$ with the boundary. The Funk metric is *not* a metric distance.

The Hilbert metric is simply the arithmetic symmetrization:

$$H_{\mathcal{C}}(x, y) = \frac{F_{\mathcal{C}}(x, y) + F_{\mathcal{C}}(y, x)}{2}.$$

It is interesting to explore clustering based on the Funk geometry, which we leave as a future work.

References

1. Agresti, A.: *Categorical Data Analysis*, vol. 482. Wiley, New Jersey (2003)
2. Aggarwal, C.C., Zhai, C.X.: *Mining Text Data*. Springer Publishing Company, Berlin (2012)
3. Messing, R., Pal, C., Kautz, H.: Activity recognition using the velocity histories of tracked keypoints. In: *International Conference on Computer Vision*, pp. 104–111. IEEE (2009)
4. Murphy, K.P.: *Machine Learning: A Probabilistic Perspective*. The MIT Press, Cambridge (2012)
5. Chaudhuri, K., McGregor, A.: Finding metric structure in information theoretic clustering. In: *Conference on Learning Theory (COLT)*, pp. 391–402 (2008)
6. Lebanon, G.: Learning Riemannian metrics. In: *Conference on Uncertainty in Artificial Intelligence (UAI)*, pp. 362–369 (2002)
7. Rigouste, L., Cappé, O., Yvon, F.: Inference and evaluation of the multinomial mixture model for text clustering. *Inf. Process. Manag.* **43**(5), 1260–1280 (2007)
8. Huang, Z.: Extensions to the k -means algorithm for clustering large data sets with categorical values. *Data Min. Knowl. Discov.* **2**(3), 283–304 (1998)
9. Arthur, D., Vassilvitskii, S.: k -means++: the advantages of careful seeding. In: *ACM-SIAM Symposium on Discrete Algorithms (SODA)*, pp. 1027–1035 (2007)
10. Gonzalez, T.F.: Clustering to minimize the maximum intercluster distance. *Theor. Comput. Sci.* **38**, 293–306 (1985)
11. Tropp, J.A.: Simplicial faces of the set of correlation matrices. *Discret. Comput. Geom.* **60**(2), 512–529 (2018)
12. Kass, R.E., Vos, P.W.: *Geometrical Foundations of Asymptotic Inference*. Wiley Series in Probability and Statistics. Wiley-Interscience, New Jersey (1997)
13. Hotelling, H.: Spaces of statistical parameters. *Bull. Amer. Math. Soc.* **36**, 191 (1930)
14. Rao, C.R.: Information and accuracy attainable in the estimation of statistical parameters. *Bull. Calcutta Math. Soc.* **37**(3), 81–91 (1945)
15. Rao, C.R.: Information and the accuracy attainable in the estimation of statistical parameters. *Breakthroughs in Statistics*, pp. 235–247. Springer, New York (1992)
16. Stigler, S.M.: The epic story of maximum likelihood. *Stat. Sci.* **22**(4), 598–620 (2007)
17. Amari, Si: *Information Geometry and Its Applications*. Applied Mathematical Sciences, vol. 194. Springer, Japan (2016)
18. Calin, O., Udriste, C.: *Geometric Modeling in Probability and Statistics*. Mathematics and Statistics. Springer International Publishing, New York (2014)
19. Amari, Si, Cichocki, A.: Information geometry of divergence functions. *Bull. Pol. Acad. Sci.: Tech. Sci.* **58**(1), 183–195 (2010)
20. Shima, H.: *The Geometry of Hessian Structures*. World Scientific, Singapore (2007)
21. Liang, X.: A note on divergences. *Neural Comput.* **28**(10), 2045–2062 (2016)
22. Jenssen, R., Principe, J.C., Erdogmus, D., Eltoft, T.: The Cauchy–Schwarz divergence and Parzen windowing: connections to graph theory and mercer kernels. *J. Frankl. Inst.* **343**(6), 614–629 (2006)
23. Hilbert, D.: Über die gerade linie als kürzeste verbindung zweier punkte. *Mathematische Annalen* **46**(1), 91–96 (1895)
24. Busemann, H.: *The Geometry of Geodesics*. Pure and Applied Mathematics, vol. 6. Elsevier Science, Amsterdam (1955)
25. de la Harpe, P.: On Hilbert's metric for simplices. *Geometric Group Theory*, vol. 1, pp. 97–118. Cambridge University Press, Cambridge (1991)
26. Lemmens, B., Nussbaum, R.: Birkhoff's version of Hilbert's metric and its applications in analysis. *Handbook of Hilbert Geometry*, pp. 275–303 (2014)
27. Richter-Gebert, J.: *Perspectives on Projective Geometry: A Guided Tour Through Real and Complex Geometry*. Springer, Berlin (2011)
28. Bi, Y., Fan, B., Wu, F.: Beyond Mahalanobis metric: Cayley–Klein metric learning. In: *IEEE Conference on Computer Vision and Pattern Recognition (CVPR)*, pp. 2339–2347 (2015)

29. Nielsen, F., Muzellec, B., Nock, R.: Classification with mixtures of curved Mahalanobis metrics. In: IEEE International Conference on Image Processing (ICIP), pp. 241–245 (2016)
30. Nielsen, F., Muzellec, B., Nock, R.: Large margin nearest neighbor classification using curved Mahalanobis distances (2016). [arXiv:1609.07082](https://arxiv.org/abs/1609.07082) [cs.LG]
31. Stillwell, J.: Ideal elements in Hilbert’s geometry. *Perspect. Sci.* **22**(1), 35–55 (2014)
32. Bernig, A.: Hilbert geometry of polytopes. *Archiv der Mathematik* **92**(4), 314–324 (2009)
33. Nielsen, F., Sun, K.: Clustering in Hilbert simplex geometry. CoRR [arXiv: abs/1704.00454](https://arxiv.org/abs/1704.00454) (2017)
34. Nielsen, F., Shao, L.: On balls in a polygonal Hilbert geometry. In: 33st International Symposium on Computational Geometry (SoCG 2017). Schloss Dagstuhl–Leibniz-Zentrum fuer Informatik (2017)
35. Laidlaw, D.H., Weickert, J.: Visualization and Processing of Tensor Fields: Advances and Perspectives. Mathematics and Visualization. Springer, Berlin (2009)
36. Lemmens, B., Walsh, C.: Isometries of polyhedral Hilbert geometries. *J. Topol. Anal.* **3**(02), 213–241 (2011)
37. Condat, L.: Fast projection onto the simplex and the ℓ_1 ball. *Math. Program.* **158**(1–2), 575–585 (2016)
38. Park, P.S.: Regular polytopic distances. *Forum Geom.* **16**, 227–232 (2016)
39. Boissonnat, J.D., Sharir, M., Tagansky, B., Yvinec, M.: Voronoi diagrams in higher dimensions under certain polyhedral distance functions. *Discret. Comput. Geom.* **19**(4), 485–519 (1998)
40. Bengtsson, I., Życzkowski, K.: Geometry of Quantum States: An Introduction to Quantum Entanglement. Cambridge University Press, Cambridge (2017)
41. Nielsen, F.: Cramér–Rao lower bound and information geometry. *Connected at Infinity II*, pp. 18–37. Springer, Berlin (2013)
42. Chapman, D.G.: Minimum variance estimation without regularity assumptions. *Ann. Math. Stat.* **22**(4), 581–586 (1951)
43. Hammersley, H.: On estimating restricted parameters. *J. R. Stat. Society. Ser. B (Methodol.)* **12**(2), 192–240 (1950)
44. Nielsen, F., Sun, K.: On Hölder projective divergences. *Entropy* **19**(3), 122 (2017)
45. Nielsen, F., Nock, R.: Further heuristics for k -means: the merge-and-split heuristic and the (k, l) -means. [arXiv:1406.6314](https://arxiv.org/abs/1406.6314) (2014)
46. Bachem, O., Lucic, M., Hassani, S.H., Krause, A.: Approximate k -means++ in sublinear time. In: Proceedings of the Thirtieth AAAI Conference on Artificial Intelligence, pp. 1459–1467 (2016)
47. Nielsen, F., Nock, R.: Total Jensen divergences: definition, properties and k -means++ clustering (2013). [arXiv:1309.7109](https://arxiv.org/abs/1309.7109) [cs.IT]
48. Ackermann, M.R., Blömer, J.: Bregman clustering for separable instances. *Scandinavian Workshop on Algorithm Theory*, pp. 212–223. Springer, Berlin (2010)
49. Manthey, B., Röglin, H.: Worst-case and smoothed analysis of k -means clustering with Bregman divergences. *J. Comput. Geom.* **4**(1), 94–132 (2013)
50. Endo, Y., Miyamoto, S.: Spherical k -means++ clustering. *Modeling Decisions for Artificial Intelligence*, pp. 103–114. Springer, Berlin (2015)
51. Nielsen, F., Nock, R., Amari, S.: On clustering histograms with k -means by using mixed α -divergences. *Entropy* **16**(6), 3273–3301 (2014)
52. Brandenburg, R., König, S.: No dimension-independent core-sets for containment under homothetics. *Discret. Comput. Geom.* **49**(1), 3–21 (2013)
53. Panigrahy, R.: Minimum enclosing polytope in high dimensions (2004). [arXiv:cs/0407020](https://arxiv.org/abs/cs/0407020) [cs.CG]
54. Saha, A., Vishwanathan, S., Zhang, X.: New approximation algorithms for minimum enclosing convex shapes. In: ACM-SIAM Symposium on Discrete Algorithms (SODA), pp. 1146–1160 (2011)
55. Nielsen, F., Nock, R.: On the smallest enclosing information disk. *Inf. Process. Lett.* **105**(3), 93–97 (2008)

56. Sharir, M., Welzl, E.: A combinatorial bound for linear programming and related problems. *STACS* **92**, 567–579 (1992)
57. Welzl, E.: Smallest enclosing disks (balls and ellipsoids). *New Results and New trends in Computer Science*, pp. 359–370. Springer, Berlin (1991)
58. Nielsen, F., Nock, R.: Approximating smallest enclosing balls with applications to machine learning. *Int. J. Comput. Geom. Appl.* **19**(05), 389–414 (2009)
59. Arnaudon, M., Nielsen, F.: On approximating the Riemannian 1-center. *Comput. Geom.* **46**(1), 93–104 (2013)
60. Bădoiu, M., Clarkson, K.L.: Smaller core-sets for balls. In: *ACM-SIAM Symposium on Discrete Algorithms (SODA)*, pp. 801–802 (2003)
61. Nielsen, F., Hadjeres, G.: Approximating covering and minimum enclosing balls in hyperbolic geometry. *International Conference on Networked Geometric Science of Information*, pp. 586–594. Springer, Cham (2015)
62. Bădoiu, M., Clarkson, K.L.: Optimal core-sets for balls. *Comput. Geom.* **40**(1), 14–22 (2008)
63. Bachem, O., Lucic, M., Krause, A.: Scalable and distributed clustering via lightweight coresets (2017). [arXiv:1702.08248](https://arxiv.org/abs/1702.08248) [stat.ML]
64. Nielsen, F., Nock, R.: On approximating the smallest enclosing Bregman balls. In: *Proceedings of the Twenty-Second Annual Symposium on Computational Geometry*, pp. 485–486. ACM (2006)
65. Nock, R., Nielsen, F.: Fitting the smallest enclosing Bregman ball. *ECML*, pp. 649–656. Springer, Berlin (2005)
66. Deza, M., Sikirić, M.D.: Voronoi polytopes for polyhedral norms on lattices. *Discret. Appl. Math.* **197**, 42–52 (2015)
67. Körner, M.C.: *Minimum hyperspheres*, Springer Optimization and Its Applications, vol. 51. Springer, New York (2011)
68. Reem, D.: The geometric stability of Voronoi diagrams in normed spaces which are not uniformly convex (2012). [arXiv:1212.1094](https://arxiv.org/abs/1212.1094) [cs.CG]
69. Foertsch, T., Karlsson, A.: Hilbert metrics and Minkowski norms. *J. Geom.* **83**(1–2), 22–31 (2005)
70. Cencov, N.N.: *Statistical Decision Rules and Optimal Inference*. Translations of Mathematical Monographs, vol. 53. American Mathematical Society, Providence (2000)
71. Cena, A.: Geometric structures on the non-parametric statistical manifold. Ph.D. thesis, University of Milano (2002)
72. Shen, Z.: Riemann-Finsler geometry with applications to information geometry. *Chin. Ann. Math. Ser. B* **27**(1), 73–94 (2006)
73. Khosravifard, M., Fooladivanda, D., Gulliver, T.A.: Confliction of the convexity and metric properties in f -divergences. *IEICE Trans. Fundam. Electron. Commun. Comput. Sci.* **90**(9), 1848–1853 (2007)
74. Dowty, J.G.: Chentsov's theorem for exponential families (2017). [arXiv:1701.08895](https://arxiv.org/abs/1701.08895) [math.ST]
75. Doup, T.M.: *Simplicial Algorithms on the Simplotope*, vol. 318. Springer Science & Business Media, Berlin (2012)
76. Vernicos, C.: Introduction aux géométries de Hilbert. *Séminaire de théorie spectrale et géométrie* **23**, 145–168 (2004)
77. Arnaudon, M., Nielsen, F.: Medians and means in Finsler geometry. *LMS J. Comput. Math.* **15**, 23–37 (2012)
78. Papadopoulos, A., Troyanov, M.: From Funk to Hilbert geometry (2014). [arXiv:1406.6983](https://arxiv.org/abs/1406.6983) [math.MG]